

CHALMERS



Dynamic model of a bubbling fluidized bed boiler

Master's Thesis in the Innovative and Sustainable Chemical Engineering

MATTIAS JOHANSSON

Department of Chemical and Biological Engineering
Division of Chemical Reaction Engineering
CHALMERS UNIVERSITY OF TECHNOLOGY
Göteborg, Sweden 2012
Master's thesis 2012:NN

MASTER'S THESIS IN INNOVATIVE AND SUSTAINABLE CHEMICAL
ENGINEERING

Dynamic model of a bubbling fluidized bed boiler

MATTIAS JOHANSSON

Department of Chemical and Biological Engineering
Division of Chemical Reaction Engineering
CHALMERS UNIVERSITY OF TECHNOLOGY
Göteborg, Sweden 2012

Abstract

The scope of this project is to create a model of a dynamic bubbling fluidized bed boiler in Dymola. The model must be able to run in real time as it will be used for operator training. The created model is limited to the gas side in the boiler up to the super heater, the other equipment already exist in Solvina's database. An extensive literature survey is done on what kind of fuels that is used for solid fuel combustion, the combustion process, largest types of boilers for solid fuels and how they work. Research is also done on how to model the different areas of bubbling fluidized bed combustion. As the model should be able to run in real time the model theory is focused on how to model each area using simplified fluid dynamics.

The formulated model uses simplified reaction kinetics, fast reactions are considered instantaneous and slow reactions are modeled with kinetics. Some of the combustion is modeled using empirical correlations only. The fluid dynamics is highly simplified, the bed is modeled as an ideally mixed tank and the freeboard area as a tank series. Heat and mass transfer as well as many other areas are modeled using correlations and semi-empirical models developed specifically for fluidized bed combustion.

Simulations of the model show that it yields realistic dynamic and steady state behavior. It is fast enough to run at real time and can therefore be implemented with other objects in Solvina's databases. Important aspects of the model have been validated against experimental values found in literature. Comparison of the model with a real bubbling fluidized bed boiler show that it is possible to adapt it to follow the behavior of an existing unit.

Although the model should be good enough to use for operator training, it contains some drawbacks that limits its use for extensive process optimization. The modeling of the emissions of sulfur dioxide and nitrogen oxide is crude, making exact predictions difficult. The neglect of the bubble phase in the bed is also a drawback that decreases the accuracy of the model.

Acknowledgement

This master thesis was performed at Solvina AB. I would like to thank the following people for all invaluable help during the exam work.

- Andreas Johansson, my advisor at Solvina, for all invaluable help with Dymola and all ideas and discussions regarding the modeling and report writing.
- Veronica Olesen, my co-advisor at Solvina, for making the report understandable and for help with the modeling.
- Bengt Andersson, my examiner, for support and help.

Content

1. Introduction	1
1.1. Scope.....	1
2. Theory	2
2.1. Solid fuels used in boilers	2
2.1.1. Coal.....	2
2.1.2. Renewable solid fuels	3
2.2. The process of combustion for solid fuels	4
2.3. Boilers for solid fuel combustion	5
2.3.1. Grate fired boiler	5
2.3.2. Fluidized bed boiler	5
2.4. Dymola	10
3. Modeling theory of a bubbling fluidized bed boiler	11
3.1. Types of models.....	11
3.2. Hydrodynamics of a fluidized bed.....	11
3.2.1. Modeling a bubbling fluidized bed.....	12
3.3. Heat transfer in bubbling fluidized bed boiler	14
3.3.1. Heat transfer between inert solid phase and gas phase in the bed	14
3.3.2. Heat transfer between fuel particles and the bed	15
3.3.3. Heat transfer between bed, walls and immersed heat exchangers.....	15
3.3.4. Heat transfer modeling in the freeboard area	17
3.4. Mass transfer resistance	19
3.4.1. Outer mass transport resistance between gas and fuel particle	19
3.4.2. Inner mass transport resistance inside the char particles	20
3.5. Fragmentation and attrition of the fuel particle	21
3.6. Fuel combustion modeling	22
3.6.1. Fuel properties	22
3.6.2. The process of devolatilization.....	24
3.6.3. Volatiles combustion	24
3.6.4. Nitrogen oxide emissions	25
3.6.5. Sulfur dioxide emissions	27
3.6.6. Char combustion.....	28
4. Method	32

4.1.	Modeling the bubbling fluidized bed.....	32
4.1.1.	The bed	32
4.1.2.	The freeboard.....	35
5.	Simulation of the boiler model.....	38
5.1.	Varying the air to fuel ratio	38
5.2.	Varying the boiler load	41
5.3.	Verification of temperatures and heat transfer	44
5.4.	Verification of bed load and emissions	45
5.5.	Model comparison with existing boiler; the Riskulla CHP	46
6.	Discussion	49
6.1.	Main difficulties during modeling	49
6.1.1.	Fast kinetics	49
6.1.2.	Emission of nitrogen oxide.....	49
6.1.3.	Emission of sulfur dioxide.....	50
6.1.4.	Bubble phase	50
6.1.5.	Radiation in the freeboard	50
6.2.	Overall model performance	51
7.	Conclusions	52
8.	References	53
	Appendix I – Investigation of reaction kinetics	59
	Appendix II – Freeboard radiation modeling	61
	Appendix III – Emission of nitrogen oxide	62

Notations

Name	Description	Unit
Roman letters		
A	Outer axial area of freeboard volume slice	m^2
A_{sh}	Mass percent of ash in fuel	%
A_c	Cross sectional area of the bed	m^2
A_{proj}	Projected area of object	m^2
A_r	Pre exponential factor for char reactions	m/sK
a_{dev}	Factor for calculation of devolatilization time	-
C	Mass percent of carbon in fuel	%
C	Concentration	mol/m^3
C_D	Air friction coefficient	-
C_p	Heat capacity	J/kgK
D_{eff}	Effective internal diffusion coefficient	m^2/s
D_g	Gas diffusion coefficient	m^2/s
D_{pore}	Pore diffusion coefficient	m^2/s
d	Diameter	m
$E_{gas-wall}$	Radiative heat exchange between gas and wall	W
$E_{i,0}$	Elutriation rate constant at bed surface	kg/m^2s
$E_{i,\infty}$	Elutriation rate constant above TDH (transport disengaging height)	kg/m^2s
E_r	Activation energy for char reactions	J/mol
f_{H_2O}	Pressure correction factor for gas emissivity	-
f_T	Factor for calculation of heat transfer coefficient between bed and char	-
f_b	Bubble fraction at wall	-
f	Factor for calculation of bubble void fraction	-
g	Gravity	m/s^2
\dot{H}	Total enthalpy flux	W
H_b	Bed height	m
H	Mass percent of hydrogen in fuel	%
HHV	Higher heating value	J/kg
ΔH_r	Heat of reaction	J/mol
h	Heat transfer coefficient	W/m^2K
h_x	Height above bed bottom	m
$h_{bed-wall}$	Total heat transfer coefficient between bed and immersed surfaces	W/m^2K
$h_{emulsion}$	Heat transfer coefficient between bed and wall from emulsion, based on emulsion contact area	W/m^2K
$h_{particles}$	Heat transfer coefficient between bed and wall from particles, based on bed contact area	W/m^2K
h_{rad}	Radiative heat transfer coefficient from bed to immersed cooling surfaces	W/m^2K
$J_{D,mf}$	Chilton-Colburn J-factor	-
K_{b-e}	Mass transfer coefficient between bed and emulsion	kg/m^3s
K_c	Thermal conductivity of a cluster of particles	W/mK
K_c	Mass transfer coefficient	m/s
K_{eq}	Equilibrium constant for the reversible water-gas shift reaction	-
K_p	Effective thermal conductivity of particles	W/mK
k_{rev}	Rate constant for the reversible water-gas shift reaction	-
k	Heat conductivity	W/mK

k	Rate constant	1/s
L	Characteristic length	m
M	Molar mass	kg/mol
\dot{m}	Component mass flow	kg/s
m	Parameter for calculation of mass transfer between bed and char	-
n	Factor for calculation of heat transfer coefficient between bed and char	-
N_s	Number of particles	-
N	Mass percent of nitrogen in fuel	%
O	Mass percent of oxygen in fuel	%
Δp_b	Pressure drop	Pa
$Q_{rad,tot,i}$	Net radiative heat exchange between slice i and the other slices	W
R	Ideal gas constant	J/molK
r	Rate of reaction	mol/m ³ s
S	Mass percent of sulfur in fuel	%
$S(t)$	Active lime surface area	m ²
S_0	Initial active surface area of the lime particles	m ²
S_V	Particle outer area to volume ratio	m ⁻¹
S_a	Particle outer area to mass ratio	m ² /kg
T	Temperature	K
T_{eb}	Effective bed temperature	K
t_X	Time for devolatilization to occur to X percent	s
V	Volume	m ³
VM^*	Volatile matter content in fuel for use in fluidized bed combustion	-
VM_0	Volatile matter content in fuel for powders under rapid heating	-
v	Velocity	m/s
X_{CaCO_3}	Calcium carbonate content in limestone	-
X_{dev}	Fraction of the devolatilization that has occurred	-
X_n	Mass percent of nitrogen in fuel	%
Y_{O_2}	Mass percent of oxygen in outlet flue gases	%
Y	Outlet concentration of sulfur dioxide	ppmv

Greek letters

ε	Void fraction; Emissivity	-
ε_{H_2O}	Gas emissivity contribution from water	-
ε_{CO_2}	Gas emissivity contribution from carbon dioxide	-
ε_g	Gas emissivity	-
$\Delta\varepsilon$	Emissivity correction factor for emissivity overlap	-
ρ	Density	kg/m ³
η	Efficiency factor for internal mass transport resistance	-
μ	Viscosity	Pas
ν	Stoichiometric coefficient	-
σ	Stefan-Boltzmann constant	W/m ² K ⁴
$\sigma(t)$	Fractional active surface area of lime particles	-
σ_{avg}	Average fractional active surface area	-
σ_c	Parameter based on pore cross sectional area variation	-
τ	Residence time	s
τ_c	Tortousity of pores	-
τ_{max}	Maximum residence time of lime particles in the bed	-
τ_p	Particle packet contact time with immersed cooling surfaces	s
Φ	Thiele modulus	-

Subscripts	
<i>p</i>	Particle; Inert bed particle
<i>B</i>	Bed
<i>b</i>	Bubble; Bed
<i>s, solid</i>	Solid phase; Particle phase
<i>f</i>	Fluid
<i>mf</i>	At minimum fluidization velocity
<i>t</i>	Terminal
<i>i, j, k</i>	Index for eg. slice number
<i>c</i>	Cross sectional
<i>0</i>	At bed surface; Initial value
∞	above TDH (transport disengaging height)
<i>e</i>	Emulsion phase
<i>g</i>	Gas phase
<i>c, char</i>	Char phase; Char particle
<i>tube</i>	Based on tube diameter
<i>conv</i>	Convective
<i>eb</i>	Effective bed
<i>w, wall</i>	Wall
<i>rad</i>	Radiative
<i>coal</i>	Coal
<i>MSW</i>	Municipal waste
<i>biomass</i>	Biomass
<i>dev</i>	Devolatilization
<i>outer</i>	Outer
<i>inner</i>	Inner
<i>eff</i>	Effective
<i>r</i>	Reaction
<i>HX</i>	Heat exchanger
<i>freeboard</i>	Freeboard, region above bed
<i>axial</i>	1D, in axial direction only
<i>net</i>	Net effect

	Dimensionless numbers	Definition	Definition (ratio of)
Bi	Biot number	$\frac{d_p h}{k_p}$	$\frac{\text{Internal heat transfer resistance}}{\text{External heat transfer resistance}}$
Re	Reynolds number	$\frac{Lv\rho}{\mu_f}$	$\frac{\text{Inertial forces}}{\text{Viscous forces}}$
Nu	Nusselt number	$\frac{hd_p}{k_f}$	$\frac{\text{Convective heat transfer}}{\text{Conductive heat transfer}}$
Pr	Prandtl number	$\frac{C_p \mu_f}{k_f}$	$\frac{\text{Viscous diffusion rate}}{\text{Thermal diffusion rate}}$
Ar	Archimedes number	$\frac{gL^3 \rho_f (\rho_s - \rho_f)}{\mu^2}$	$\frac{\text{Boyancy force}}{\text{Inertial force}}$

Sh	Sherwood number	$\frac{K_c d_p}{D_g}$	$\frac{\text{Convective mass transfer}}{\text{Diffusive mass transfer}}$
Sc	Schmidt number	$\frac{\mu_f}{\rho_f D_g}$	$\frac{\text{Viscous diffusion rate}}{\text{Mass diffusion rate}}$

1. Introduction

A large part of the world's supply of energy comes from burning of solid fuels in boilers and furnaces [1] [2]. While oil and natural gas prices are high and production is likely to have peaked, the prices are significantly lower for coal and the reserves are enormous [1] [2] [3]. Although carbon dioxide taxes are decreasing the building rate of new coal fired heat and power plants in developed countries, they are rapidly built in developing countries [1].

In developed countries the usage of biomass in energy production is increasing. This is to lower the release of greenhouse gases and to lower the dependence on fossil fuels [1]. In Sweden burning of biomass is commonly used in industries for steam production and in municipals for district heating [4]. Burning of municipal waste is also increasing, due to more strict regulation on waste dumping in many countries and for economical reasons [3]. All of these examples illustrate the increased usage of solid fuels in boilers.

How these boilers are operated greatly affect the efficiency and emission from the boiler and its operation is therefore a crucial aspect to maximize plant efficiency and minimize emissions. By using simulation models of the boiler the operator can test different operating conditions and gain a deeper understanding of the boiler. New operators can train handling different scenarios and the simulator could even be used for optimizing the operating conditions. Experimenting with the real boiler could lead to costly production disturbances.

Although several models for solid fuel boilers exist in literature, most of them are too computationally costly to be used for real time simulations and most of them can only be used to find steady state solutions.

The goal of this project to create a model of a boiler for solid fuels in the simulation software Dymola. The model must not be too complex, as it should be possible to use it for real time simulations, but still accurate enough to capture the dynamics and behavior of the boiler at different operating conditions with different fuels.

The type of boiler that will be modeled is a bubbling fluidized bed. These have become very popular due to its many advantages, see section 2.3.2. Many bubbling fluidized beds have been built and it is likely to continue to be a popular boiler type.

1.1. Scope

A short list will be presented describing the scope and limitations of the project.

- Modeling focus on one specific boiler, a bubbling fluidized bed boiler.
- The model must not be too complex, as it should be possible to perform real time simulations.
- The model should be dynamic.
- Only the flue gas side of the firebox and not the complete boiler including equipment such as heat exchangers or external flue gas treatment etc will be modeled.
- The model must be able to handle inputs from all types of fuel, including biomass, waste and coals.

2. Theory

This section will handle subjects important for the simulation of a boiler for solid fuels. These include the types of solid fuels available and their specific combustion behavior, a description of the combustion process for solid fuels and the type of boilers used for solid fuel combustion. A short theory section about the modeling program will be presented as well.

2.1. Solid fuels used in boilers

There are a wide variety of solid fuels available for use in different types of boilers. A rough division can be made between coal and renewable fuels [3].

2.1.1. Coal

Coal is a type of sediment rock formed from dead plant matter. It is developed through a process of oxygen free decomposition at elevated pressures [3]. Due to continuous sedimentation on the organic matter there is a pressure build-up, leading to both dewatering and compactisation. In the early stages of these processes water, carbon dioxide and nitrogen are released from the matter while in later stages mainly methane is released [3]. The first material formed is peat, followed by lignite (soft brown coal), bituminous coals (stone coal) and anthracites.

Coal is mainly composed of carbon, but also other components like hydrogen, oxygen, sulfur, nitrogen and various mineral components. The age of the coal has a strong influence on its properties, with younger coals having a significantly higher volatiles and moisture content compared to older coals [5]. Coal is one of the most abundant sources of energy, existing in far greater quantities than oil and natural gas [1]. It is the largest energy source for electricity production worldwide, even though the coal usage for energy applications in Sweden is very low [1] [4].

There exist numerous classifications of coal between different countries, classifying coal according to its volatiles content, calorific value or moisture content. One classification is by the American Society for Testing and Materials (ASTM). This classification is shown in Table 1 [5].

Table 1, classification of coals according to ASTM standard. Older coals are classified by volatile content while younger coals are classified by their calorific value. All values are on a dry, mineral matter free basis [5].

Group	Subgroup	Volatile content [%]	Calorific value [MJ/kg]
Anthracite	Meta anthracite	0-2	-
	Anthracite	2-8	-
	Semi-anthracite	8-14	-
Bituminous coal	Low-volatile bituminous coal	14-22	-
	Medium-volatile bituminous coal	22-31	-
	High volatile bituminous coal A	31-40	> 32.6
	High volatile bituminous coal B	-	30.2-32.6
	High volatile bituminous coal C	-	26.7-30.2
Subbituminous coal	Subbituminous coal A	-	24.2-26.7
	Subbituminous coal B	-	22.1-24.4

	Subbituminous coal C	-	19.3-22.1
Lignite	Lignite A	-	14.6-19.3
	Lignite B	-	0-14.6

Coal can either be burned as a fine powder or as larger chunks. The fine coal powder is easy to handle, burns relatively fast and boilers similar to boilers for liquid fuels can be used. The cost of grinding the coal to a powder is however expensive and only viable for very large thermal power plants. Therefore boilers that can handle larger coal chunks have been developed [3].

2.1.2. Renewable solid fuels

The renewable solid fuels can be divided into biomass, coming from agricultural areas and forests, and waste, the renewable part of the waste stream coming from human and industrial processes.

The lower heating value (combustion energy, not including condensation energy of the formed water vapor) of dry and ash free biomass is typically around 20 MJ/kg [3]. With increasing moisture content this value decreases rapidly. The moisture content of newly harvested agricultural plants are typically less than 40% while fresh wood lies in the range of 40-60% [3]. By drying the biomass the moisture content often decrease below 20% [3].

The volatiles content in biomass is significantly higher than in coals and the ash content is often much lower. Ash is typically mineral matter and other non-combustible substances. While the volatiles content in old coals often is less than 15%, the typical volatiles content in biomass is 76% for wood and 73% for straw [3]. The ash content varies with the type of biomass and the type of coal, but is typically only a few percent in wood and twice as much in agricultural biomass [3]. While coals contain significant amounts of sulfur, the content in biomass is often very low. The chloride content in biomass can however often be high, making the biomass ash much more corrosive than coal ash [3].

The ash softening (where the ash start to deform) and melting temperatures differ significantly between different fuel sources. For older coals, the softening temperature is often above 1200°C, while for some types of straw it can be as low as 750°C which can cause problems in some types of boilers [6]. For most types of biomass (especially wood) the ash softening temperature is above 900°C [3].

Three common types of waste are the household waste, the sewage sludge waste and the industrial waste [3]. Industrial wastes are often relatively homogeneous and of high quality, making it easy to burn. Household waste on the other hand is often a mixture of organics, burnable synthetic materials, metals, glass and other non-combustible materials. The lower heating value of household waste differ between different countries depending on consumption behaviors and recycling, in Sweden the lower heating value is 9-13 MJ/kg [3].

Due to a very high moisture content sewage sludge are mechanically dewatered before combustion, reducing the water content from about 96% to around 60% [3]. The sludge may

also be thermally dried before combustion. Due to the high water content and high ash content (typically around 30-50%) the lower heating value of sewage sludge lie around 1-3 MJ/kg [3].

2.2. The process of combustion for solid fuels

The process of combustion of solid fuels in an oxygen containing atmosphere can be divided into three steps; drying, devolatilization and char burning. For small fuel particles the temperature is uniform throughout the particles and all three processes occur sequentially [7]. For larger solids the temperature gradient throughout the solid can be significant and all processes occur simultaneously [7]. Whether the processes occur simultaneously or sequentially can be found by calculating the Biot number, see eq. (1) [7].

$$Bi = \frac{d_p \cdot h}{k_p} \quad (1)$$

For Biot numbers much less than one, the internal temperature gradients are small, while for high Biot numbers, the heat transport to the surface of the particle is higher than the internal heat conduction [7]. This results in a temperature wave from the surface to the centre of the particle with the processes of drying, devolatilization and char combustion following as the temperature increases [7].

The extent of moisture in solid fuels differ significantly, with biomass having a very high moisture content and coal having a much lower moisture content. During drying the solid is first heated to the evaporation temperature of the water and then all moisture in the particle is evaporated. For biomass the high moisture content require significant amounts of energy for evaporation. This decreases the usable energy output from biomass, if the heat of condensation in the flue gases is not recovered.

When the particle has dried the temperature increase and the solid fuel starts to decompose, releasing volatile substances. This process is called devolatilization [7]. The volatiles consist mainly of light hydrocarbons like methane together with carbon dioxide, carbon monoxide, hydrogen and water vapor. Significant amount of tars (heavy hydrocarbons) can also be produced, but are usually quickly oxidized to lighter products [8]. During devolatilization the volatile products ignite and form a flame around the particle consuming all oxygen close to the particle, thus preventing char burning [7]. The flame heats the particle further, increasing temperature and devolatilization rate until all volatiles are consumed [7]. During biomass pyrolysis, hemicelluloses are the first substances to pyrolyze, followed by cellulose and lignin. During coal pyrolysis, younger coals like lignite start to pyrolyze at lower temperatures compared to older coals like anthracite [7].

After the devolatilization only highly porous char remains and the char combustion starts. The solid get highly porous from the loss of materials during drying and devolatilization and because of this the oxygen can easily penetrate the fuel [7]. Depending on combustion conditions and fuel the combustion occurs either equally over the whole particle, increasing the porosity of the particle further or at the surface of the particle, decreasing its diameter [7].

Char combustion is highly exothermic and the particles get a significantly higher temperature compared to the surrounding gas. The process of char combustion takes significantly longer time compared to the processes of drying and devolatilization [6].

2.3. Boilers for solid fuel combustion

Solid fuels are either burned directly (wood logs or chips, chunks of coal) or milled into a fine powder (sawdust, coal powder). The size of the fuel particles greatly impact the combustion characteristics and the type of boiler used. For powders the fuel can be injected directly and mixed with air for combustion, similarly to liquid and gaseous fuels. For larger solids the most common types of boilers are the grate fired boiler and the fluidized bed [7]. Only boilers burning larger solids will be treated here, as these are the most interesting to model.

2.3.1. Grate fired boiler

The grate fired boiler is one of the oldest systems for burning solid fuels. It can either have a fixed or a moving bed, with a moving bed more common for larger units. With a moving bed the solid fuel is fed onto a sloping and moving grate, driving the fuel further into the boiler [7]. The capacity of grate fired boilers is relatively low, from less than one MW thermal effect and up to about 150 MW thermal [3]. In many areas the grate fired boiler has been replaced with either boilers using coal powder or by fluidized bed boilers. However one application still dominated by grate fired boilers is for waste incineration [3]. Two common types of grate fired boilers are the Spreader Stoker and the Traveling Grate Stoker, both of the moving bed type.

In the Traveling Grate Stoker fuel is fed from one end onto a circulating belt. Air is blown from below through the fuel layer on the belt, resulting in drying, pyrolysis and char burning as the belt moves [7]. Supplementary air is injected above the grate giving a complete combustion of all fuel gases. The air blown from below also serves to cool the belt and can therefore not be preheated to very high temperatures [3]. This type of boiler is suitable for fuels with a narrow particle size distribution, if the fuel contains fines these may fall down through the belt leading to boiler losses [3]. The combustion can take very long due to the formation of an ash layer around the particle hindering oxygen penetration. This makes the fuel residence time very long.

For fuels containing fines, a Spreader Stoker is often more appropriate. In this the fuel is thrown out on the bed, causing small fines to ignite and burn even before landing on the bed [3]. Due to elutriation (small particles following the gas flow) the fly ashes is often recycled to the bed as they still contain combustible char [3].

2.3.2. Fluidized bed boiler

Fluidized bed combustion was originally developed for combustion of coals with high sulfur content. The formed sulfur dioxides can easily be neutralized by addition of limestone into the bed [6]. The boiler is excellent for burning low value fuels and has a great advantage as it can burn several different fuels at once [6]. The characteristic feature of the fluidized bed combustion compared to conventional boilers is that the combustion takes place in a fluidized bed of inert solid material. The fluidization is created by the upward flow of combustion air. The operating temperature of a fluidized bed boiler is narrow, around 800-900°C. Lower

temperatures lead to decreased boiler efficiency while a too high temperature can lead to ash sintering, causing the bed to clog [6].

In contrast to the grate-fired boilers where the bed consists solely of fuel, most of the bed in a fluidized bed boiler consists of inert material with a fuel content of only a few percent [7]. The most common types of fluidized bed boilers are the bubbling fluidized bed boiler (the boiler that will be modeled) and the circulating fluidized bed boiler [3]. The fluidization regime of the boiler is determined by the fluidization velocity, these regimes are explained in the next section.

2.3.2.1. Regimes of gas-solid fluidization

The regimes of a gas-solid mixture can be classified into the following categories; fixed bed, bubbling bed, turbulent bed, fast fluidization and pneumatic transport. A schematic figure of these regimes is illustrated in Figure 1, along with the characteristic pressure drop over the bed at the specific regime.

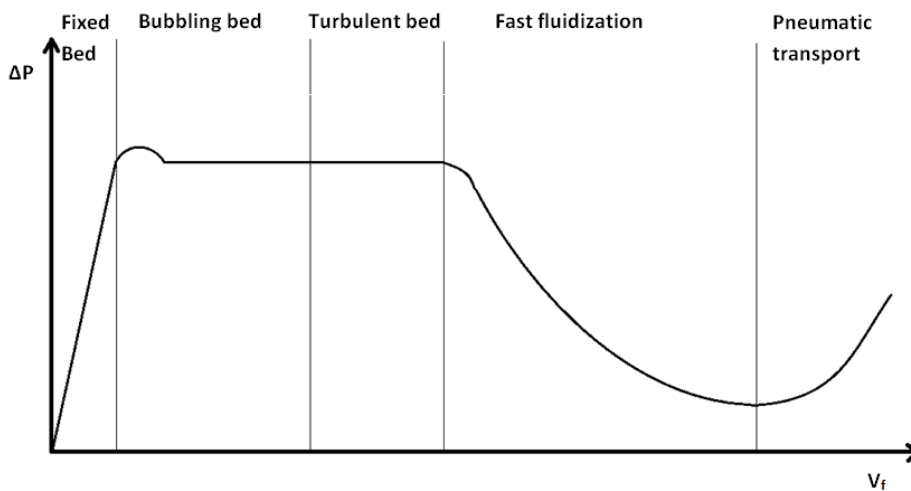


Figure 1, schematic view of the pressure drop for different fluidization regimes for a fluidized bed, characterized by the gas velocity [6].

From Figure 1 it is clear that the pressure drop increase with increasing gas velocity until the onset of fluidization and thereafter maintain a constant value, equal to the weight of the bed [3]. The small peak of the pressure drop at the onset of fluidization is due to the presence of adhesive forces between the particles, which disappear as the particles begin to move [6]. With velocities slightly above minimum fluidization velocity, bubbles begin to form and the bed can be considered to be composed of two phases; the emulsion phase with solids and gas at fluidization and the bubble phase, which is almost free of particles [6]. The bubbles contribute largely to the mixing of the bed, with particles flowing upwards in the wake of the bubbles and particles flowing downwards around the bubbles and at the walls. When bubbles reach the surface they burst, hurling particles far above the bed [6].

As the gas velocity is increased the bubbling bed is expanding and finally reaches the turbulent fluidization regime where larger bubbles are split into smaller and irregularly shaped voids and the bed starts to homogenize [6]. The transition from bubbling to turbulent bed

takes place gradually as the velocity is increased and an exact limit can be hard to determine [6].

By further increasing the fluidization velocity the bed reaches the so called fast fluidization regime where the number of particles entrained in the flow abruptly increases. During this regime a large part of the particles are entrained in the flow, even though many fall back as they come further up in the boiler [6]. This backward flow of solid particles creates a very intense mixing and large solid-gas interaction and some units are therefore designed to operate in this regime, these are called circulating fluidized beds. As many particles escape the boiler during this fluidization regime a large recirculation is needed as the whole bed otherwise will be transported out of the boiler [6].

At even higher velocities the back-flow of particles ceases and the particles move uniformly upwards with the gas flow without any strong particle-particle interaction. This flow regime is called pneumatic transport [6].

2.3.2.2. *Bubbling fluidized bed*

The bubbling fluidized bed work in the bubbling regime. Because of the relatively low rate of fluidization, almost no solids are entrained in the flow and the need for solids recirculation is low [6]. However many boilers use fly ash recirculation, as some unburned char often escape with the fly ash, to increase the boiler efficiency [6]. Due to the low fluidization velocity the bed has a clearly defined bed surface, which is not found in boilers working in the fast fluidization regime. The walls of the bed are usually covered with water tubes recovering heat from the bed. In some cases this cooling is not enough to keep the bed temperature at 800-900°C and immersed heat exchangers are used also [6]. The heat transfer in the bed part of the boiler is high, mainly due to the inert fluidized particles while the heat transfer in the region above the bed is lower than in conventional boilers due to lower temperatures [3]. A schematic figure of a bubbling fluidized bed boiler is shown in Figure 2 [6].

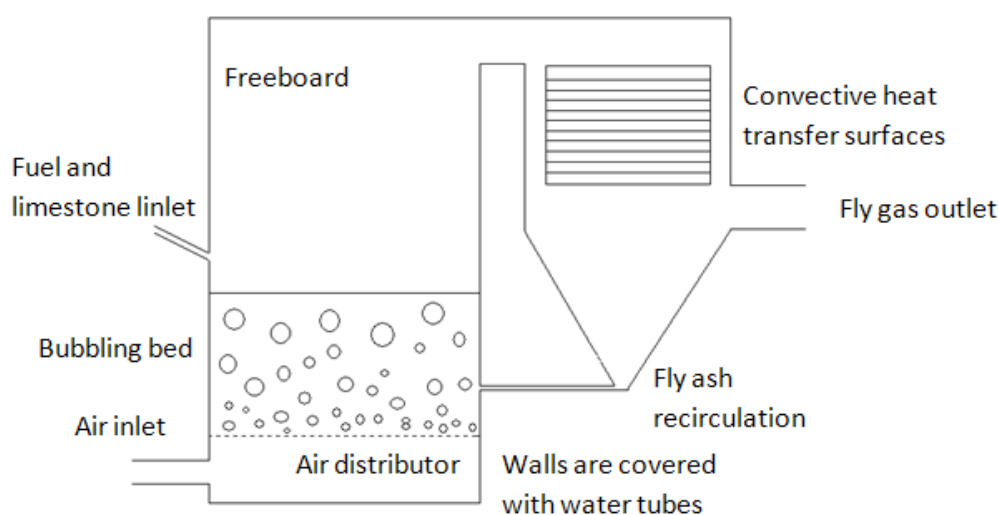


Figure 2, bubbling fluidized bed boiler with major parts labeled. In the bubbling fluidized bed the bubbles and the emulsion phase can be distinguished.

The fuel can be fed to the bed in two different ways, depending on the fuel properties. For larger particles, reactive coals and biomass, the fuel is fed on top of the bed [3]. This gives an even distribution of the fuel over the bed. For smaller particles and less reactive fuels, the fuel is fed directly into the bed. This does not give as good fuel distribution as over bed feeding, but the fuel entrainment is minimized [3].

The region over the bed is called the freeboard, and is almost free of solid particles. In this region any residual volatiles are burned. Due to the presence of bubbles in the bed, some of the oxygen may not be available for the combustion. In the turbulent flow over the freeboard this residual oxygen is mixed with the rest of the gas flow, burning any residual volatiles [9]. For reactive coals and biomass this can lead to a flame appearing on top of the bed, making the temperature in the initial part of the freeboard higher than in the bed [9]. When staged air flow is used the temperature in the freeboard can be significantly higher than in the bed.

The greatest advantage of bubbling fluidized bed combustion boilers over conventional boilers is the possibility to burn fuels of low quality and high ash or moisture content [3]. Bubbling fluidized beds can burn fuels with up to 60% moisture and up to 70% ash [6]. It can burn all types of fuel ranging from coal, biomass of different kinds, domestic waste and industrial waste. The typical boiler efficiency is 90% without fly ash recirculation and over 98% including fly ash separation [6]. Reactive fuels are easily burnt while some high equality coals are harder, yielding lower efficiencies [6].

Due to the lower operating temperature of the boiler, the flue gas emissions of nitrous oxides are significantly lower than in conventional boilers [6]. By addition of limestone into the bed the sulfur content of the fuel is significantly reduced, removing the need for after treatment of the flue gases for sulfur oxides [6]. This gives a clear economic advantage to the fluidized bed boilers compared to conventional boilers. To further reduce the emissions of nitrous oxides, some of the air can be injected above the bed, lowering the oxygen concentrations in the bed and thereby the amount of nitrous oxides formed.

One of the shortcomings of the bubbling fluidized bed is a relatively low horizontal mixing rate in the bed [6]. While the vertical mixing is very good, the horizontal is significantly lower. Because of this a high number of feed points are needed for fuels to be fed below the bed surface [6]. For very large boilers the number of feed points needed can be substantial, resulting in that very large fluidized bed boilers are unpractical to build [6]. Another shortcoming is the relatively high recirculation ratio of fly ash needed to achieve high combustion efficiencies (up to 5:1). Another major disadvantage is the large corrosion present in the bed resulting from the fluidized particles.

The turndown ratio (boiler load) of a fluidized bed is usually not that good, lower gas velocities does not lower the heat transfer to the water tubed walls enough to compensate for much lower fuel inputs. To improve turndown ratio of fluidized bed combustion boilers the fluidized bed can be divided into several compartments, allowing only some of them to be utilized at lower loads [6].

2.3.2.3. Circulating fluidized bed boiler

The circulating fluidized bed boiler is a relatively new technique. The first commercial boilers were built during the 1980s and were developed to overcome some of the basic disadvantages with bubbling fluidized beds [6].

In circulating fluidized beds the gas velocity is significantly higher compared to bubbling fluidized beds. In the lower part of the furnace the conditions are similar to bubbling fluidized beds while higher up in the boiler the differences are momentous. The gas velocity is higher than the particle free fall velocity resulting in a significant flow of particles with the gas. Many of them fall back higher up in the furnace, causing very high vertical and horizontal mixing and large heat exchange with the gas phase [6]. Exiting gas is led to a cyclone separating the particles from the gas. The inert particle size is considerably smaller than those in bubbling fluidized beds, around 50-300 μm , compared to 0.5-2 mm [6]. Due to the intensive circulation, the high heat transfer and high heat capacity of the solids the temperature is constant throughout the boiler [6]. While combustion and heat transfer is high in the bed section of a bubbling fluidized bed, the whole boiler is utilized in the circulating fluidized bed [6]. A schematic figure of a circulating fluidized bed boiler is shown in Figure 3 [3].

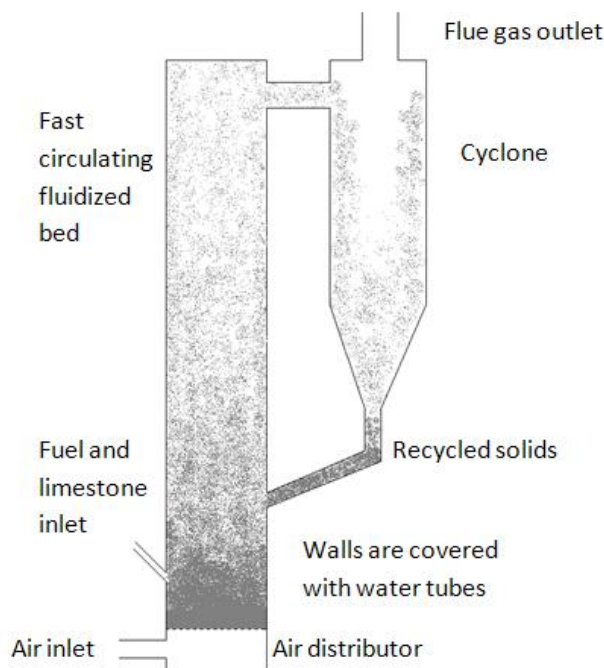


Figure 3, circulating fluidized bed boiler with major parts labeled

Circulating fluidized beds have smaller cross sectional area and are higher compared to bubbling fluidized beds, see Figure 3. This combined with the fact that the mixing is stronger decreases the need for many fuel injection points. Therefore it is easier to build large circulating fluidized beds [3].

As the fuel is recirculated until complete combustion (except for small amounts not separated by the cyclone) the combustion efficiency is very high, typically 99.5% [6]. The high and uniform temperature throughout the boiler also increases the sulfur dioxide reduction, making it much higher than in bubbling fluidized beds [6].

By changing the recirculation rate of solid particles the load of the boiler can easily be controlled. A lower recirculation rate significantly decreases the heat transfer to the water tubed walls and allows turndown ratios of up to 1:5 [6]. The bed, or lower part of the boiler is usually covered with fire proof bricks and there are no immersed heat exchangers inside the boiler. This significantly decreases the corrosion inside the boiler [6].

One of the disadvantages of the circulating fluidized bed is that it requires smaller fuel and lime particles, making fuel preparation more expensive. Lime stone particles should not exceed 0.5 mm while fuel particles should be below 10 mm. The boiler itself also has a higher consumption of electricity compared to a bubbling fluidized bed decreasing the boiler efficiency [6].

2.3.2.4. Comparison of bubbling and circulating fluidized bed boilers

As conclusion bubbling fluidized beds are superior for low and medium capacity boilers up to about 50 MW thermal effect [6]. They are good for fuels with higher volatile content, like biomass or low grade coals and for less strict environmental regulations [6]. The circulating fluidized bed is a more complex boiler and is suitable for higher loads, for burning of fuel with less volatiles and with more strict environmental regulation [6]. Lastly, fluidized bed combustion boilers are superior to all other boiler techniques for burning of low quality solid fuels [6].

2.4. Dymola

The boiler model is built in the modeling and programming software Dymola. Dymola is an object oriented programming tool with a standard library and with the possibility of creating new objects. It is useful for handling large, complex and dynamic systems with multiple layered objects. Dymola uses automatic formula manipulation which minimizes the need for manual equation manipulation [10]. The programming is based on the programming code Modelica. Models can be built from already existing objects or new objects can be created by switching to the programming view.

The programming is made using a system of Differential Algebraic Equations (DAE). Different solvers are available for solving the system, where the default solver is Dassl. It can be used for solving implicit systems of algebraic equations, instead of solving them explicitly as is done with for example Euler. Using the implicit solving method more systems are possible to solve than with an explicit solver. Dassl also uses a non-fixed step method which increases the stability and possibility of finding a solution, especially for stiff systems.

3. Modeling theory of a bubbling fluidized bed boiler

In this section modeling theory for fluidized bed combustion will be described. This starts with a short introduction to different types of models, followed by a description of the hydrodynamics of a fluidized bed as well as empirical and semi-empirical correlations used to model specific features of the bed. Heat and mass transfer between phases are described in sections 3.3 and 3.4 while particle wear is described in section 3.5. The modeling of the fuel combustion is described in section 3.6.

3.1. Types of models

A large number of models of fluidized bed combustion have been published over the years. The level of detail between these models differs significantly. To get an overview of the modeling of fluidized bed combustion these models can be classified according to the level of simplification used to solve the fluid dynamics. The models can be classified into computational fluid dynamics (CFD) models, fluidization models and grey box models (advanced black box) [11].

CFD models solve the fundamental transport equations for all the phases, usually with model-specific correlations for the interaction terms between phases and for the kinetics. These models are very computationally demanding for a steady state solution and even more so for dynamic conditions. An example of a dynamic CFD model is a model presented by Chen et al [12].

A common and highly researched type of models is the one dimensional fluidization model. This model assumes that the bed consists of a bubble phase and an emulsion phase and in some cases a cloud phase surrounding the bubbles [13] [14]. The bubbles are assumed to be free of particles and moving upward in a plug flow from the bottom to the top of the bed [14]. All interaction with the emulsion phase, as well as bubble growth and coalescence are described by empirical correlations. The emulsion phase consists of gas and solid particles in a state of fluidization and is often considered to be perfectly mixed [14]. An early bubbling fluidized bed boiler model that can be classified as a fluidization model was developed by Sarofim and Beer [15]. More comprehensive models of this type have been developed for example by Gomez-Barea and Leckner [11], by Souza-Santos [13] [14] and by Oka [6].

The grey box models consist of overall mass, heat and momentum balances for the fluidized bed. As kinetics is involved, the bed is usually modeled as a perfectly mixed tank. Equilibrium relations can also be used instead of real kinetics to describe the composition in the reactor [11]. An example of a dynamic grey box model of a bubbling fluidized bed boiler is given by Surasani et al. [9].

In this project a grey box model is created using many correlations and relationships from the 1D fluidization models. This is to create a model that is simple enough for real time simulation but accurate enough to correctly predict the boiler performance.

3.2. Hydrodynamics of a fluidized bed

Most of the differences between regular solid fuel combustion units and a fluidized bed combustion boiler arise from the presence of an inert fluidized solid phase [6]. The presence

of this phase has a substantial impact on the combustion characteristics and is therefore important to understand.

The solid phase in a fluidized bed combustion boiler does not consist of a single type of material, but the inert (often sand) is mixed with other solids like coal/biomass, char, ash from the fuel and limestone for sulfur emissions control [11]. These solids often have a size distribution ranging over a large interval of sizes. During modeling a single particle size is however often assumed for each solid [6]. Another common assumption is that of spherical particles. The actual sphericity typically ranges from 0.6-0.9 for the most commonly used materials [6].

3.2.1. Modeling a bubbling fluidized bed

At the onset of fluidization, the pressure drop equals the weight of the bed. This fact can be used to calculate the onset of fluidization by combining the Ergun equation, eq. (2) [16], with a pressure balance of the fixed bed, eq. (3). Combining this with the experimentally found data by Wen and Yu in eq. (4) [17] gives a correlation for the minimum fluidization velocity, eq. (5).

$$\Delta p_B = H_B \frac{150(1 - \varepsilon)^2 \mu_f v_f}{\varepsilon^3 \phi_s^2 d_p^2} + H_B \frac{1.75(1 - \varepsilon) \rho_f v_f^2}{\varepsilon^3 \phi_s d_p} \quad (2)$$

$$\Delta p_B = (1 - \varepsilon)(\rho_p - \rho_f)gH_B \quad (3)$$

$$\frac{1}{\phi_s \varepsilon_{mf}^3} \approx 14 \quad \text{and} \quad \frac{1 - \varepsilon_{mf}}{\phi_s^2 \varepsilon_{mf}^3} \approx 11 \quad (4)$$

$$Re_{mf} = \frac{d_p v_{mf} \rho_f}{\mu_f} = (33.7^2 + 0.0408 Ar)^{0.5} - 33.7 \quad (5)$$

Another important parameter is the maximum fluidization velocity where entrainment starts to occur. The maximum fluidization velocity is given by eq. (6), the definition of the Reynolds number (see Notations) and the friction coefficient for a spherical particle, given in Table 2.

$$C_D Re_t^2 = \frac{4}{3} Ar \left[1 - 1.2(1 - \varepsilon)^{\frac{2}{3}} \right]^2 \quad (6)$$

Table 2, the friction coefficient for a spherical particle.

Range of Reynolds numbers	Friction coefficient, C_D
0 – 2	$C_D = 24/Re$
2 – 500	$C_D = 18.5/Re^{0.6}$
500 – $2 \cdot 10^5$	$C_D = 0.44$

It is important to take the polydispersity (size variation) of the solids into account. It will decrease the feasible velocity range for the gas phase making it relatively narrow [6].

As the velocity increase above the minimum fluidization velocity the bed will expand further, the expansion can be found by calculating the porosity of the bed. An expression for the porosity at velocities above the minimum fluidization velocity is given by eq. (7) [6].

$$\varepsilon = \varepsilon_{mf} \left[\frac{Re + 0.02Re^2}{Re_{mf} + 0.02Re_{mf}^2} \right]^{0.1} \quad (7)$$

In a fluidized bed particle elutriation, loss of particles from the bed, will always occur. The main causes for this are particle attrition (see section 3.5) and bubble bursting at the surface, giving some particles a very high velocity [18]. Particles with a free fall velocity higher than the gas velocity will always fall back into the bed if the freeboard region is sufficiently high [18]. Particles with a free fall velocity lower than the gas velocity will however always follow the gases out of the boiler. The height at which particles at a certain size start to fall back to the bed can be calculated. One estimate of the so called transport disengaging height can be found from calculating the elutriation rate constants, eq. (8) [19] and (9) [18], and defining the transport disengaging height as the height at which the mass flow rate of particles out of the reactor has reached 99% of its value at infinite height, eq. (10) [18].

$$\frac{E_{i,\infty}}{\rho_f(v_f - v_t)} = 4.6 \cdot 10^{-2} \left(\frac{(v_f - v_t)^2}{gd_p} \right)^{0.5} Re_p^{0.3} \left(\frac{\rho_p - \rho_f}{\rho_f} \right)^{0.15} \quad (8)$$

$$E_0 = 0.3d_b d_p^{-1.17} (v_f - v_{mf})^{0.66} \quad (9)$$

$$TDH_i = \frac{1}{4} \ln \left\{ \frac{E_0 - E_{i,\infty}}{0.01E_{i,\infty}} \right\} \quad (10)$$

The bubbles in a fluidized bed are created near the gas distributor plate at the bottom of the bed and rise upwards in a vertical manner to the top of the bed [14]. Depending on the type of solid material in the bed the bubbles can rise quickly with almost no mass exchange with the surrounding emulsion phase, causing some of the incoming air to bypass the bed, or rise slowly with good mass exchange with the emulsion phase [6]. The bubbles grow and become larger due to coalescence as they rise through the bed. For beds with high height/diameter ratio, plug flow may occur, causing very different bed characteristics compared to bubbling fluidized beds [6].

The velocity of a single rising bubble may be calculated using an analogy to rising bubbles in a liquid, eq. (11), as these processes are similar [20].

$$v_{b,\infty} = 0.711\sqrt{gd_b} \quad (11)$$

The bubble diameter depends on how far from the distributor plate the bubble has traveled. For a bed material with larger particles of the size typically used in fluidized bed combustion, eq. (12) can be used to calculate the bubble diameter [11].

$$d_b = 0.54(v_f - v_{mf})^{0.4} (h_x + 4A_c^{0.5})^{0.8} g^{-0.2} \quad (12)$$

For a real fluidized bed the presence of other bubbles increase the velocity of the bubble due to wake formation behind the bubble, a better estimation of the bubble velocity is therefore given by eq. (13) [6].

$$v_b = v_{b,\infty} + (v_f - v_{mf}) \quad (13)$$

The bubble void fraction in the bed can be found from eq. (14) and (15) [11].

$$\varepsilon_b = \left[1 + \left(\frac{1.3}{f} \right) (v - v_{mf})^{-0.8} \right]^{-1} \quad (14)$$

$$f = [0.26 + 0.7 \exp(-3.3d_p)] [0.15 + (v - v_{mf})]^{-\frac{1}{3}} \quad (15)$$

The mass transfer coefficient for mass transfer between the bubble and emulsion phase can be determined from eq. (16) [11]. It takes into account both convective and diffusive mass transfer.

$$K_{b-e} = \frac{2v_{mf}}{d_p} + \frac{12(D_g \varepsilon_{mf} v_b)^{\frac{1}{2}}}{\pi d_b^{\frac{3}{2}}} \quad (16)$$

3.3. Heat transfer in bubbling fluidized bed boiler

In fluidized bed combustion there are a number of heat transfer processes that usually are included in a model. These are heat transfer between the gas and the inert solid phase, the heat transfer between the fuel and gas phase and heat transfer between the bed and immersed cooling surfaces [6].

3.3.1. Heat transfer between inert solid phase and gas phase in the bed

The temperature in a fluidized bed is almost completely homogeneous due to the intensive mixing occurring with the inert material. Even with an operating temperature at 800-900°C, incoming air at ambient temperature and highly exothermic reactions occurring in the gas phase the temperature difference between the gas phase and solid phase is rarely more than a few degrees [6]. The low temperature difference is due to the high heat transfer that exists between the solid particles and the gas phase, mainly due to the very high contact area [6]. The solid phase has a very large heat capacity compared to the gas and therefore stabilizes the bed temperature, evening out any fluctuations in gas inlet temperature or fuel quality.

The standard correlation for heat transfer between a gas and a single particle is according to equation (17) [6].

$$Nu_p = 2 + 0.74 Re_p^{0.5} Pr^{0.33} \quad (17)$$

This correlation is however inferior when applied to a fluidized bed. An empirical correlation developed for fluidized beds, also taking into account axial dispersion, by Gunn is found in equation (18) [21].

$$Nu_p = (7 - 10\varepsilon + 5\varepsilon^2)(1 + 0.7Re_p^{0.2}Pr^{0.33}) + (1.33 - 24\varepsilon + 12\varepsilon^2)Re_p^{0.7}Pr^{0.33} \quad (18)$$

This equation is valid for $0.35 < \varepsilon < 1$ and $Re_p > 15$.

3.3.2. Heat transfer between fuel particles and the bed

After the cold fuel particle is injected into the bed, the particle is heated to evaporation temperature and moisture is evaporated. When all moisture is evaporated, the particle temperature increases and the processes of devolatilization and thereafter char burning takes place [14]. During drying and devolatilization heat is transferred to the particle while heat is transferred from the particle during the char combustion. When the particle is ignited the particle temperature can be significantly higher than in the surrounding gas and inert solid [9]. As the fuel load in a fluidized bed usually is very low, 2-5 wt%, any fuel-fuel particle interaction can be neglected [6] [7].

The heat transfer between the fuel particles and the bed is by gas convection, particle contact and radiation. Particle radiation has not been sufficiently researched and is therefore often neglected [6]. For fuel particles at the same size or smaller than the inert particles the convective heat transfer is most important while particle contact has major impact for large fuel particles. The heat transfer coefficient between fuel particle and bed is dependent on the fluidization velocity and show a maximum value at the optimal fluidization velocity. The maximum heat transfer increases with a decrease in fuel particle size [6]. Equation (19) show a correlation for the maximum heat transfer coefficient at optimal fluidization velocity [6].

$$Nu_{max}Ar^{-n} = \frac{3.539}{f_T} \left(\frac{d_c}{d_p} \right)^{-0.257} \quad (19)$$

Where n and f_T is given by eq. (20) and (21) respectively.

$$n = 0.105 \left(\frac{d_c}{d_p} \right)^{0.082} \quad (20)$$

$$f_T = 0.844 + 0.0756 \left(\frac{T_b}{273} \right) \quad (21)$$

The correlation is made for inert particles of diameters from 131 μm to 1010 μm , fuel particle diameters of 4 mm to 20 mm and bed temperatures up to 900°C [6].

3.3.3. Heat transfer between bed, walls and immersed heat exchangers

One of the characteristic features of fluidized beds is the greatly enhanced heat transfer to immersed walls and heat exchangers. This is mainly due to the much larger heat capacity and mobility of the solid phase compared to a homogeneous gas phase [6]. The heat transfer mechanisms in fluidized beds are very complex, but can be divided into heat transfer by particle motion and contact, gas convection by gas in bubbles and gas in the emulsion phase

and heat transfer by radiation [6]. At bed temperatures below 600-700°C the heat transfer due to radiation can be neglected. The most important properties that determine the intensity of the heat transfer is the fluidization velocity and the particle size [6].

A mechanistic way of modeling the heat transfer, called the packet-renewal model, is presented by Basu [22]. The heat transfer is divided into three parts, particle convection, gas convection and radiation. The largest contribution to the heat transfer is given by the particle convection [22].

According to the packet-renewal model, clusters of particles at bed temperature are swept to the wall surface by action of the bubbles [22]. These clusters stay in contact with the wall for a certain time before being swept away and replaced by another cluster of particles. During the particle-wall contact the particles are transferring heat by conduction to the tube covered wall. The particle conduction is made up of contributions from the bubble and the emulsion phase. Because of the low particle concentration in the bubble phase, this contribution is only a fraction of the contribution from the emulsion and is often neglected [22]. Neglecting the bubble phase contribution the particle convective heat transfer coefficient can be written according to eq. (22) [22].

$$h_{particle} = (1 - f_b)h_{emulsion} \quad (22)$$

The fraction of tube surface covered by bubbles, f_b , is given by eq. (23) [22].

$$f_b = 0.08553 \left[\frac{(v - v_{mf})^2}{gd_p} \right]^{0.1948} \quad (23)$$

The convective heat transfer of the emulsion phase is modeled as two resistances in series, the contact resistance, R_w , and the packet resistance, R_c . The contact resistance is the heat transfer resistance between the bed and outer particles in the cluster. The packet resistance is the resistance within the cluster. An empirical factor derived from experiments is used to take overlap between the resistances into account. The emulsion heat transfer coefficient is given by eq. (24) [22]. The resistances are shown in eq. (25) and (26) [22].

$$\frac{1}{h_{emulsion}} = R_w + 0.45R_c \quad (24)$$

$$R_w = \frac{d_p}{3.75K_c} \quad (25)$$

$$R_c = \sqrt{\frac{\pi \tau_p}{K_p \rho_p C_{p,p}}} \quad (26)$$

The contact time, τ_p , is given by eq. (27) [22].

$$\tau_p = 8.932 \left[\frac{gd_p}{(v - v_{mf})^2} \right]^{0.0756} \sqrt{\frac{d_p}{0.025}} \quad (27)$$

The effective thermal conductivity, K_p , is obtained by eq. (28) and the thermal conductivity of the cluster, K_c , is given by eq. (29) [22].

$$K_p = K_c + 132d_p v_{mf} \rho_p C_{P,g} \quad (28)$$

$$K_c = k_p \left\{ 1 + \frac{(1 - \varepsilon_{mf}) \left(1 - \frac{k_f}{k_p}\right)}{\left[\frac{k_f}{k_p} + 0.025 \varepsilon_{mf}^{0.63} \left(\frac{k_f}{k_p}\right)^{0.18} \right]} \right\} \quad (29)$$

The gas convective component of the bed-wall heat transfer component can be calculated by eq. (30) for $Re_{tube} < 2000$ and by eq. (31) for $Re_{tube} > 2000$ according to Basu [22].

$$Nu_{conv} = 0.05 Re_{tube} Pr \quad (30)$$

$$Nu_{conv} = 0.18 Re_{tube}^{0.8} Pr^{0.33} \quad (31)$$

The radiative component of the bed-wall heat transfer component is given by eq. (32). According to Basu the effective bed temperature should be taken as 85% of the bulk temperature due to the lower particle temperature close to the cooling surface [22].

$$h_{rad} = \frac{\sigma(T_{eb}^2 + T_w^2)(T_{eb} + T_w)}{\frac{1}{\varepsilon_b} + \frac{1}{\varepsilon_w} - 1} \quad (32)$$

The total bed-wall heat transfer coefficient is given by eq. (33).

$$h_{bed-wall} = h_{particles} + h_{conv} + h_{rad} \quad (33)$$

Various experimental correlations for heat transfer to immersed surfaces also exist, where the correlation presented by Wen and Leva in [23] and the correlation by Zabrodsky et al. presented in [24] yield good predictions according to Oka [6].

3.3.4. Heat transfer modeling in the freeboard area

The heat transfer intensity in the freeboard is significantly lower due to the very low particle concentration. The main transfer mechanisms are by gas convection and by radiation [22]. The temperature profile over the freeboard can differ significantly depending on the type of fuel and bed conditions [6]. For high volatile fuels a large part of the devolatilization gases may burn in the freeboard region, causing flames to appear. Because of this, the temperature in the freeboard may be higher than the bed temperature [6]. Typically the temperature drop along the freeboard due to the continuous cooling from the water tubed walls.

The axial heat transport in the freeboard is not only by flow, but also by radiation as large temperature gradients can exist in the gas [25]. As the emissivity of the bed is very high, and its temperature often is higher than the gas in the freeboard, a significant heat transport from the bed may also occur, see section 4.1.2.1.

There are several different approaches to modeling the radiation in a furnace, some of the more important are described by Mishra et al. [26]. One popular method is the zonal model where the furnace is discretized into cells, both axially and radially. View factors between each block is calculated and from this the radial exchange can be found, this model is described in several articles [27] [28].

Bueters et al. developed an axial radiative exchange model based on slicing the furnace gas volume into cells in the flow direction, see Figure 4 [29]. The model is based on a grey body emissivity model of the gas with an exponential decay of the radiation intensity with length from the radiation source [29]. Dounit et al. modeled axial radiation using this model but with a somewhat different formulation, shown in eq. (34) [25] [30].

$$Q_{rad,tot,i} = \varepsilon_{g,i}(E_{i-1} + E_{i+1}) + \sum_{j=1}^{j=i-2} \left(E_j \varepsilon_{g,i} \prod_{k=i-1}^{j+1} (1 - \varepsilon_{g,k}) \right) + \sum_{j=i+2}^N \left(E_j \varepsilon_{g,i} \prod_{k=i+1}^{j-1} (1 - \varepsilon_{g,k}) \right) \quad (34)$$

The total radiation from a slice i , E_i , is given by eq.(35).

$$E_i = \varepsilon_{g,i} \sigma A T_i^4 \quad (35)$$

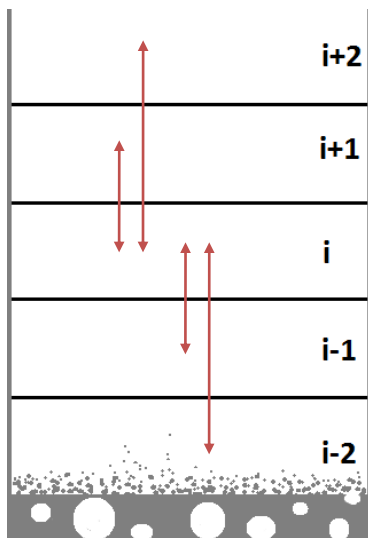


Figure 4, discretized freeboard region. The arrows show the axial radiative exchange calculated by eq. (34). Each slice has a unique temperature and emissivity.

The gas emissivity depends on the characteristic radiative length as well as the content of absorbing gases, mainly water and carbon dioxide. The emissivity is usually calculated from the so called Hottel charts [31]. In these charts the individual emissivities of carbon dioxide and water and correction factors for pressure deviations and spectral overlap are given as functions of temperature, characteristic radiation length and partial pressure [31]. These are then combined into a total emissivity, see eq. (36).

$$\varepsilon_g = f_{H_2O} \varepsilon_{H_2O} + \varepsilon_{CO_2} - \Delta\varepsilon \quad (36)$$

The characteristic length is defined according to eq. (37).

$$L = 3.6 \frac{V}{A_{proj}} \quad (37)$$

Mehrotra et al. have fitted these Hottel charts according to empirical equations to allow for use in computer simulations, these equations are not presented here but can be found in [31]. Bahadori et al. have made a similar but less extensive correlation for the gas emissivity, this can be found in [32].

Heat transfer to the walls in the freeboard is by gas convection and radiation. As the particle concentration in the freeboard of a bubbling fluidized bed is low, particle entrainment is neglected [22]. According to Basu, eq. (30) and eq. (31) can be used to describe the heat transfer due to gas convection in the freeboard [22]. The radiative heat transfer to the walls can be modeled by a radiative heat exchange equation, see eq. (38) [6].

$$E_{gas-wall} = \frac{A_{wall} \sigma (T_g^4 - T_{wall}^4)}{\frac{1}{\varepsilon_g} + \frac{1}{\varepsilon_{wall}} - 1} \quad (38)$$

3.4. Mass transfer resistance

Both outer mass transfer resistance to the particle and inner mass transfer resistance in the particle may be significant in a fluidized bed boiler. In this section correlations are described to take the inner and outer mass transport resistance into consideration.

3.4.1. Outer mass transport resistance between gas and fuel particle

For the char combustion reactions (see Section 3.6.6) significant outer mass transfer resistance can occur at the high combustion temperature of the char particles.

The mass transfer to fuel particles in a fluidized bed is significantly lower compared to the mass transfer around a free sphere due to the hindrance from the other particles. A simple expression for the mass transfer analogous to eq. (17) is given in eq. (39) [6].

$$Sh = (2 + 0.69Re^{0.5}Sc^{0.33})\varepsilon \quad (39)$$

The ratio of fuel particle diameter to inert solid particle diameter has a significant effect on the mass transfer and this is not taken into consideration by eq. (39) [6]. For fuel sizes close to the size of the inert material, eq. (39) can be used. An increase in the inert material size yields a higher mass transfer rate due to the increase in minimum fluidization velocity while an increase in fuel particle size yields a lower mass transfer rate, probably due to an increase in boundary layer size around the particle [6]. Higher fluidization velocities seem to have no effect on the mass transfer and calculations can therefore be conducted for minimum fluidization velocity [6]. Eq. (40) gives a correlation for the mass transport when the ratio of the particle diameters is not close to unity [6].

$$\varepsilon_{mf} j_{D,mf} Re_{mf}^m = 0.105 + 1.505 \left(\frac{d_c}{d_p} \right)^{-1.05} \quad (40)$$

Where m is given by eq. (41) and j_D by eq. (42) [6].

$$m = 0.35 + 0.29 \left(\frac{d_c}{d_p} \right)^{-0.5} \quad (41)$$

$$j_D = \frac{k_c}{v_f} Sc^{2/3} \quad (42)$$

The correlation is based on experiments with fuel particle diameters from 4 mm to 20 mm and fuel to inert particle diameter ratios of about 5 to 200.

3.4.2. Inner mass transport resistance inside the char particles

The effect of inner mass transfer can be taken care of by the use of an efficiency factor in the rate expression. This efficiency factor can be calculated according to eq. (43) assuming the particles are spherical and the reaction is first order (which is usually assumed for char combustion) [36].

$$\eta = \frac{3}{\Phi^2} (\Phi \coth \Phi - 1) \quad (43)$$

Where Φ represent the Thiele modulus, which for a first order reaction and spherical particle is defined according to eq. (44) [33].

$$\Phi = \frac{d_c}{2} \sqrt{\frac{k_{\text{char kin.}} S_V}{D_{\text{eff}}}} \quad (44)$$

The effective diffusion inside the particle can be calculated according to eq. (45) [33].

$$D_{\text{eff}} = \frac{D_{\text{pore}} \varepsilon_p \sigma_c}{\tilde{\tau}} \quad (45)$$

For large pores the pore diffusivity can be approximated with the gas diffusivity while for small pores, less than 1 μm , the Knudsen diffusion coefficient can be used, see eq. (46) [34].

$$D_{pore} = 1.534 * 10^{-3} d_{pore} \sqrt{\frac{T}{M_A}} \quad (46)$$

3.5. Fragmentation and attrition of the fuel particle

The processes of fragmentation and attrition (wear) are important during modeling as they can increase the number and decrease the size of fuel particles in the fluidized bed [35]. When fuel particles enter the boiler they are subject to extreme temperature gradients, strong mechanical action from the inert solids and internal pressure from the fast devolatilization process creating gases inside the particle [35].

Fragmentation processes are divided into groups depending on their physical nature. Fragmentation due to thermal stresses and due to internal pressure increase is called primary fragmentation. Char particle fragmentation due to internal burning and decrease in porosity is called secondary fragmentation and the mechanical stress on the particles from the inert material producing fines are called attrition [6].

With primary fragmentation, the fuel particle may swell and/or fragment during devolatilization depending on properties of the fuel [35]. Due to very intense heating of the particle the devolatilization may be very violent leading to a rapid pressure increase inside the particle from the increase of volatiles volume. For particles with high porosity the volatiles can escape the particle while for particles with lower porosity the devolatilization will lead to swelling and/or fragmentation of the particle [35]. Whether the particle will fragment or not can be estimated using eq. (47) together with Figure 5 [35]. For values above the line the particle will most likely fragment while particles with values below the line is not probable to fragment.

$$PRN(\text{pore resistance number}) = \frac{\text{Volatiles content}}{\text{Equilibrium moisture content}} \quad (47)$$

It should be noted that the model is developed for bituminous coals and usage for other coals or biomass may not be correct [35].

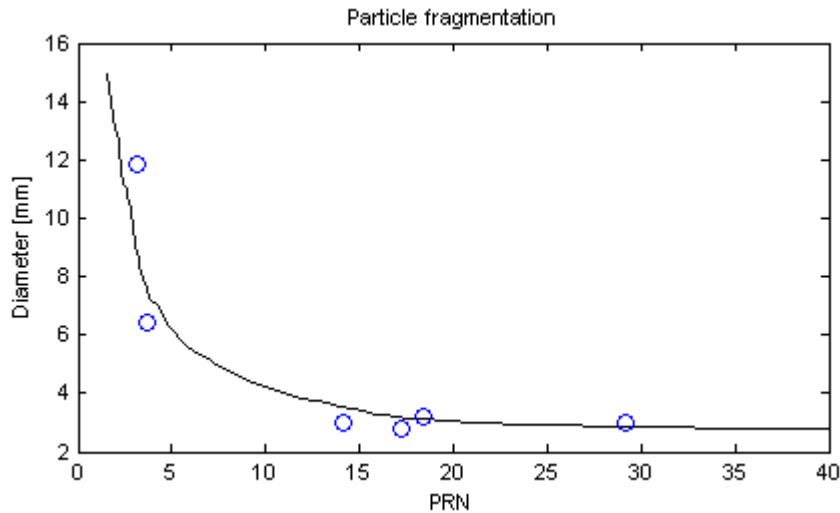


Figure 5, particle diameter given as a function of pore resistance number. Particles above the line are likely to fragment while particles under the line are not likely to fragment [35].

The process of attrition is the process of formation of very small char particles due to mechanical stress from the inert solid particles. These small particles are small enough to be elutriated out of the boiler before complete burnout, which can lead to significant boiler losses [6]. While not all particles suffer from primary or secondary fragmentation, attrition is always present in a fluidized bed boiler. The attrition of a burning fuel particle is much faster than attrition of an inert particle with the same mechanical strength. This is due to the continuous formation of cracks and surface roughness from the heterogeneous reactions taking place on the fuel particle [36].

3.6. Fuel combustion modeling

Combustion is a complex phenomenon including a large number of reactions, especially with solid fuels. To accurately model combustion in a fluidized bed the devolatilization process, along with char burning and burning of the light gases and tars produced during devolatilization, needs to be understood and modeled. Drying of the particle is usually considered very fast and will therefore not be included here [6]. Emission for nitrogen oxide and sulfur dioxide will also be discussed and modeled.

3.6.1. Fuel properties

Basic properties of the fuel may not always be known, this section aims at giving some basic relations for determining fuel properties from the elemental composition of the fuel. The section is divided into coal fuels and renewable fuels.

3.6.1.1. Coal

A table over coal elemental compositions for a large number of American coals is given by Anthony et al. [37]. This table can be used to estimate the elemental composition if this is not known, based on the classification of the coal.

The heat of combustion for a coal fuel is an important parameter. It can be calculated according to eq. (48), if the elemental composition is known. The correlation was developed by Neavel et al. by multivariate analysis of numerous coals [38]. The elemental compositions

are given in wt% dry (ash containing) basis and the heat of combustion is given on a dry basis.

$$HHV_{fuel} = 2326(145.9C + 569.6H - 53.89O + 43.08S - 6.3Ash) \quad (48)$$

Another important coal property is the volatile matter content. Although the volatiles content is dependent on the specific conditions in the boiler and on the particle size and type, see Section 3.6.2, an estimate of the volatiles content can be found using eq. (49), developed by Neavel et al. for devolatilization of coal powder under rapid heating to 900°C [38].

$$VM_0 = -0.408[C] + 11.25[H] + [O] + 1.3[S] \quad (49)$$

The concentrations are in wt% dry (not ash free) basis. Experiments carried out by Merick [39] in a fluidized bed show that the volatile content usually is lower than predicted by eq. (49) and a better estimate of the release of volatiles in a fluidized bed may be given by eq. (50) [39].

$$VM^* = VM_0 - 0.36VM_0^2 \quad (50)$$

It should be noted that the above equation is established for bituminous coal and may not give accurate results for other types of fuel.

The coal density can be estimated by eq. (51), also developed by Neavel et al. The components are given in wt%.

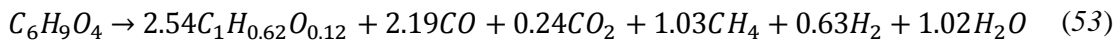
$$\rho_{coal} = 15.56C - 41.17H + 22.47O + 20.49S + 20.8Ash \quad (51)$$

3.6.1.2. Renewable fuel

Other equations need to be used for prediction of renewable fuel properties. An estimation of the higher heating value for wood and plant material is given in eq. (52). by Friedl et al [40]. Compositions are given in wt% dry and heating value in kJ/kg.

$$HHV_{biomass} = 3.55C^2 - 232C - 2230H + 51.2C \cdot H + 131N + 20600 \quad (52)$$

From experiments, Tepper established the hypothetical formula for dry biomass to $C_6H_9O_4$ and biochar to $C_1H_{0.62}O_{0.12}$. Based on the work by Tepper, the pyrolysis formula described in eq. (53) was created by Surasami [8] [9]. It can be used to estimate the relation between volatiles and char in biomass.



The properties of municipal waste differ from the properties of wood and plant biomass, see Section 2.1.2. An equation for prediction of the higher heating value from elemental composition of the municipal waste is given in eq. (54), developed by Kathiravale et al. [41]. Compositions are given in wt% dry and heating value in kJ/kg.

$$HHV_{MSW} = 416.6C - 570H + 259O + 599N - 5829 \quad (54)$$

3.6.2. The process of devolatilization

The mass fraction of volatiles in a fuel varies greatly, with coal volatiles content typically 10 – 50 wt% [6] and biomass volatiles content typically 70 – 80 wt% [42]. The amount of volatiles released is not only dependent on the fuel type but also depend on the conditions at which the devolatilization occurs. Because of this, no exact estimation of the volatiles content can be made solely from the chemical composition of the fuel. During devolatilization a large number of chemical species are created, both gaseous and tars (liquids) [7]. Tars will in turn decompose into gaseous compounds and char [8]. The process of devolatilization can be divided into two regimes, at low temperature most of the volatiles are released, although only a smaller fraction of the hydrogen. Most of the hydrogen is instead slowly released in the second regime at higher temperatures [6]. The major devolatilization products are methane, water, hydrogen, carbon monoxide and carbon dioxide [7].

The process of devolatilization is very complex, involving numerous bond breaking reactions, but is also dependent on the heat transfer rate, internal temperature gradients and how easily the volatiles can escape the particle. For coal powders with very small particle diameters, below 100-200 μm , the rate of devolatilization is solely determined by the kinetics [37]. As the process is composed of numerous different reactions a mean kinetic rate is usually not good enough, but the process is instead modeled as a large number of reactions with varying activation energy [37]. The activation energies are assumed to be spread as a gaussian distribution and a standard deviation of these activation energies is experimentally determined [37]. For larger particles however, the internal mass and heat gradients can be limiting, making the diameter of the particle the most important parameter [6].

A correlation for approximation of the devolatilization time is given by Peeler et al. in eq. (55) [43]. The equation relates the devolatilization rate to the total amount of volatiles and the particle diameter.

$$t_X = \frac{2}{a_{dev} d_p^{-0.8}} VM^{*1/2} [1 - (1 - X_{dev})^{1/2}] \quad (55)$$

The expression by Peeler is based on experiments with several different coals, with volatile contents ranging from 9% to 37%. The fuel particle diameters range from about 1 mm to 30 mm and the temperature is 900°C. The parameter a_{dev} is given by eq. (56) which is a least square fit based on experimental points presented by Peeler [43].

$$a_{dev} * 10^{-3} = 1.2089 + 1.2573VM^*[\%] \quad (56)$$

The volatile matter content in eq. (56) is given on a dry and ash free basis.

3.6.3. Volatiles combustion

There are a large number of gas phase reactions occurring during solid fuel combustion. From the devolatilization process a high variety of substances are created, ranging from methane to heavy hydrocarbons (tars). For simplicity only reactions for the most important compounds are considered [8] [9]. The reactions are presented in Table 3. The first four reactions are chosen based on a similar selection made by Surasani et al. [9] while the last two

reaction are from a larger set found in a work by Tepper [8]. The other reactions in Tepper are excluded due to the very small creation of the substances involved [8].

Table 3, Homogeneous gas phase reactions considered most important during combustion [8] [9]

Reaction	Mechanism
Carbon monoxide oxidation [9]	$CO + 1/2O_2 \rightarrow CO_2$
Hydrogen oxidation [9]	$2H_2 + O_2 \rightarrow 2H_2O$
Methane partial oxidation [9]	$CH_4 + 3/2O_2 \rightarrow CO + 2H_2O$
Water-gas shift reaction [9]	$CO + H_2O \leftrightarrow CO_2 + H_2$
Tar oxidation [8]	$CH_yO_z + 1/2O_2 \rightarrow CO + zH_2O + (y/2 - z)H_2$
Catalyzed thermal tar cracking [8]	$CH_yO_z \rightarrow 2/3CO + 1/3CH_4 + (z - 2/3)H_2O + (y/2 - z)H_2$

The kinetics of the water-gas shift equilibrium reaction is presented in Table 4 [44].

Table 4, kinetics of the water-gas equilibrium reaction. The constant a_{WGS} has the value 0.333 for temperatures below 1073 K and the value 0.5 for temperatures above 1073 K [44].

K_{eq}	$\exp(-4.33 + 4577.8/T)$
$k_{rev}, T < 1073 \text{ K}$	$7.6 \cdot 10^4 \exp(-164.2 \cdot 10^3 / RT)$
$k_{rev}, T > 1073 \text{ K}$	$1.2 \cdot 10^{13} \exp(-318 \cdot 10^3 / RT)$
$r \text{ [mol/m}_{3, \text{gas}}]$	$k_{rev}(K_{eq} C_{CO}^{0.5} C_{H_2O} - C_{H_2}^{u_{WGS}} C_{CO_2})$

Kinetics for the other reactions are presented in Table 5, where the kinetics for the first three reactions are presented by Jensen et al. and the last two by Tepper et al. [45] [8]. The thermally catalyzed tar cracking reaction is catalyzed by the presence of a solid surface, here this solid is assumed to be sand. The activation energy and pre exponential factor will be different for other solids [8].

Table 5, the kinetics of the other homogeneous gas phase reactions [45] [8].

Reaction	Rate expression	Unit
Carbon monoxide oxidation	$3.25 \cdot 10^7 \exp(-15098/T) C_{CO} C_{O_2}^{0.5} C_{H_2O}^{0.5}$	$\text{mol/m}_{\text{gas}}^3$
Hydrogen oxidation	$1.631 \cdot 10^9 \cdot T^{3/2} \exp(-24157/T) C_{H_2}^{3/2} C_{O_2}$	$\text{mol/m}_{\text{gas}}^3$
Methane partial oxidation	$1.585 \cdot 10^{10} \exp(-24157/T) C_{CH_4}^{0.7} C_{O_2}^{0.8}$	$\text{mol/m}_{\text{gas}}^3$
Tar oxidation	$20700 \cdot T \exp(-80234/RT) P^{0.3} C_{tar}^{0.5} C_{O_2}$	$\text{mol/m}_{\text{gas}}^3$
Catalyzed thermal tar cracking	$0.7 \cdot (T_{ref}/T) \exp(-63100/RT) \rho_{bed} C_{tar}$	$\text{mol/m}_{\text{bed}}^3$

3.6.4. Nitrogen oxide emissions

Due to the lower temperature in fluidized bed combustion compared to conventional boilers the NO_x emissions are also lower in general [6]. According to Jensen et al. almost all of the formed nitrogen oxides is created from the nitrogen content in the fuel and almost no nitrogen oxides are created from gaseous nitrogen [45].

As in conventional boilers the amount of nitrogen oxide emissions mainly depends on the amount of excess oxygen used in the combustion process. Jensen et al. have conducted an extensive parameter study to determine the most influential parameters on nitrous oxides emission [46]. From his review it can be concluded that a low air to fuel ratio, small bed particles, low minimum fluidization velocity and low bubble-emulsion interaction yield a low outlet concentration of nitrogen oxides [46]. The main reduction reactions are the NO reduction by CO catalyzed by char and bed material and the direct oxidation of NH₃ to N₂ catalyzed by the char and bed material. Therefore a high carbon monoxide concentration, large residence time and large surface areas of char and bed material yield low NO_x emissions [46]. Another extensive review on the emissions of nitrogen oxides from fluidized bed combustion is presented by Johnson with similar conclusions as Jensen's report [47].

Existing models for NO_x emissions can roughly be divided into crude models and comprehensive models. The crude models have an empirical approach while the comprehensive models try to capture the complex reaction behavior in larger detail. Ehrlich et al. present a very crude empirical model with emission levels only dependent on temperature [48]. Another, more extensive correlation is presented by Gruhl et al. who use large amounts of experimental data to correlate the emission levels [49]. The newest correlation found is presented by Newby et al. who present an empirical correlation for the NO_x emissions from a bubbling fluidized bed without air staging, see eq. (57) [50]. The experimental conditions leading to this model are not presented in the article.

$$NO_x(ppmv) = 12.25 \exp\left(\frac{2827}{T}\right) Y_{O_2}^{0.24} X_n^{0.44} Y^{-0.1} \quad (57)$$

Y_{O_2} is the volume percent of oxygen in the reaction products, X_n is the mass percent of nitrogen in the fuel and Y is the outlet concentration of SO_2 in ppmv.

More comprehensive models have been developed to describe the reaction mechanisms in great detail. Johnsson was the first to introduce a comprehensive kinetic model incorporating a large number of reactions for the nitrogen oxide formation and retention [51]. This has been further developed by Jensen and Johnsson [45] [52]. A similar model built on data from Johnsson and Jensen is presented in several works [53] [54] [55] [56]. This model is presented in Table 6. The nitrogen content in the fuel is divided between volatile nitrogen and char bound nitrogen. The division determines the substance formed, with volatile nitrogen assumed to only form NH₃ and char bound nitrogen to only form NO. The division is determined experimentally to 79 % volatile nitrogen and 21 % char bound nitrogen for Turkish lignite.

Table 6, nitrogen reactions included in the fluidized bed combustion model.

Reaction	Place	Rate expression	Unit
$N_{vol} + 3/2H_2 \rightarrow NO + 3/2H_2O$	gas	Instantaneous	—
$N_s + 1/2O_2 \rightarrow NO$	char	Proportional to char combustion rate	mol/m^3s
$NH_3 + 5/4O_2 \rightarrow NO + 3/2H_2O$	gas	$2.21 \cdot 10^{14} \exp(-38160/T) C_{NH_3}$	mol/m^3s
$NO + 2/3NH_3 \rightarrow 5/6N_2 + H_2O$	gas	$2.45 \cdot 10^{14} \exp(-27680/T) C_{NH_3} C_{NO}$	mol/m^3s
$NO + Char \rightarrow 1/2N_2 + CO$	char	$2.62 \cdot 10^6 \exp(-22200/T) C_{NO}^{0.52}$	mol/kgs
$NO + CO \rightarrow 1/2N_2 + CO_2$	char	$1.15 \cdot 10^7 \exp(-22800/T) C_{NO}^{0.39} C_{CO}^{0.53}$	mol/kgs

$NH_3 + 3/4O_2 \rightarrow NO + 3/2H_2O$	char	$34C_{NH_3}C_{O_2}$	<i>mol/kgs</i>
$NH_3 + 3/4O_2 \rightarrow NO + 3/2H_2O$	ash	$3.33 \cdot 10^{-2} C_{NH_3}^{0.57} C_{O_2}^{0.11}$	<i>mol/kgs</i>
$NH_3 + 5/4O_2 \rightarrow 1/2N_2 + 3/2H_2O$	char	$84C_{NH_3}C_{O_2}$	<i>mol/kgs</i>
$NH_3 + 5/4O_2 \rightarrow 1/2N_2 + 3/2H_2O$	ash	$23.6C_{NH_3}^{1.8} C_{O_2}^{0.07}$	<i>mol/kgs</i>

Because of the lower temperature in fluidized beds there can be a significant formation of N_2O along with NO_x when burning coals [6]. The emission of N_2O can often be in the same order of magnitude as the emission of NO_x although their relative composition changes with several factors [6]. The temperature has the strongest effect on the relative composition of N_2O and NO_x , with NO_x rising while N_2O decreasing as the temperature is increased [6]. When burning biomass the emission of N_2O is significantly lower, often only a few ppm [6].

3.6.5. Sulfur dioxide emissions

Coal fuels often contain a certain amount of sulfur which form sulfur dioxide during combustion. Fluidized bed combustion is very good for reducing the emissions by addition of a reducing agent, often limestone [6]. Biomass often contain very low amounts of sulfur or none at all and sulfur retention is therefore not needed in case of biomass combustion.

The retention process can roughly be divided into two steps, the calcination of the limestone, see eq. (58), and the reaction between the sulfur dioxide and the burnt lime, see eq. (59) [57].



The first stage is very fast and often seen as instantaneous during modeling [57]. The second steps is however very complex as the reaction is heterogeneous and as the solid product, $CaSO_4$, has a significantly larger volume compared to the solid reactant, CaO [58]. Because of this the pores of the porous lime particle is plugged as the reaction proceeds, causing the reaction to slow down and finally stop before all lime is consumed [58] [59]. These processes make accurate modeling of the sulfur retention hard. As with the nitrous oxide emissions the models range from models trying to capture all physical steps to the simpler semi-empirical models.

One simple model trying to describe the sulfur retention is the SURE-model, originally created by Schouten and van den Bleek [57] [60] and further developed by Lin et al. [58] [59] [61]. This model takes into account the maximum possible conversion of the lime particles and the residence time distribution of the particles but has a very simple approach to the pore plugging. A model similar to the SURE-model that has been used in several works, [53] [54] [55] [56], will be presented here. The consumption rate of sulfur dioxide is given by eq. (60). As the reaction proceeds it is deactivating the outer area of the particles. This deactivation is modeled as an exponential decay with time, eq. (61) and (62) [54].

$$r_{SO_2} = -kS(t)C_{SO_2} = -kS_0\sigma(t)C_{SO_2} \quad (60)$$

$$S_0 = \frac{6M_{CaO}}{\rho_{CaO}d_p} \quad (61)$$

$$\sigma_t = \frac{S(t)}{S_0} = \exp\left(-\frac{6M_{CaCO_3}kC_{SO_2}}{X_{CaCO_3}\rho_{CaO}d_p}\right) \quad (62)$$

The average fractional active surface is found by integration of the residence time distribution with the exponential decay expression, see eq. (63) [54].

$$\sigma_{avg} = \left(1 + \frac{6M_{CaCO_3}kC_{SO_2}}{X_{CaCO_3}\rho_{CaO}d_p}\tau\right)^{-1} \left[1 - \exp\left(-\left(\frac{1}{\tau} + \frac{6M_{CaCO_3}kC_{SO_2}}{X_{CaCO_3}\rho_{CaO}d_p}\right)\tau_{max}\right)\right] \quad (63)$$

From experiments, the kinetic rate constant, k , is found to be 14.9 cm/s [54].

There exist many more advanced models for sulfur retention, using single particle models [62], taking the reactivity of the specific limestone into consideration [63] or using specialized models taking the ash and already sulfated lime into account [64] [65]. Most of these models are however too computationally demanding or complex for this work.

The accuracy of all sulfur retention models may however be questioned, a review of several sulfur retention models performed by Shih et al. show that the variation in reaction rate between different models can be several orders of magnitude [66].

3.6.6. Char combustion

Under stationary conditions relatively small amounts of char is present in the boiler, usually 2-5 wt% of the inert solids, depending mainly on char reactivity, the diameter of the char particles and air to fuel ratio [6]. The char combustion reaction is by far the slowest process. Its time constant is often an order of magnitude higher than the devolatilization process and it has therefore a large influence on the combustion [6].

Char combustion is a heterogeneous process, where oxygen has to diffuse through the gas film around the char to the surface and possibly into the char particle. Whether char oxidation occurs throughout the particle or only at the surface of the particle depend on the kinetics of char combustion, on the porosity of the char, the outer mass transport to the char and the temperature [6].

If not all reactions occur at the surface of the particle, an efficiency factor needs to be calculated, taking the inner mass transport of the particle into consideration. The true, inner reaction rate must also be used together with the inner surface area of the particle. The inner surface area of char is strongly dependent on the char origin and on the conditions under which the char was made. Typical values for coals range from 100 to 600 m²/g char [67]. The relation between inner and outer reaction rate is given in eq. (64). For calculation of the efficiency factor, see section 3.4.2.

$$r_{i,outer} = \eta \frac{S_a}{S_V} \rho_p r_{i,inner} \quad (64)$$

The true, inner reaction rate of char is still strongly dependent on the char origin, with wide variations found within the same type of char and between different chars [67]. These great differences occur partly due to impurities found in the char (ash) that can act either as inhibitor or as a catalyst for char combustion reaction [67]. An approximate reaction rate for the oxidation of char with oxygen, correlated by Smith from a huge amount of experimental data over a wide range of conditions, is shown in eq. (65) [67]. It should be noted that this equation is for the combustion of coal power, i.e. very small particles.

$$r_{char,ox} = 0.2511T \exp\left(-\frac{179.4 \cdot 10^3}{RT}\right) C_{O_2} \quad (65)$$

In fluidized beds the particles are usually quite large and the bed temperature is often around 800 – 900 °C. Under these conditions most of the char combustion reactions occur at the particle surface [6]. A typical way of modeling the char combustion reaction is therefore to assume that all reactions occur at the surface of the char particle. This gives a reaction front moving inwards, leaving an ash layer around the particle giving resistance to mass transport. This reaction may be modeled as a series of resistances, see eq. (66) [68,69].

$$r_{char,ox} = \frac{v_{stoich} C_{O_2}}{\frac{1}{k_{char\ kin.}} + \frac{1}{k_{mass, film}} + \frac{1}{k_{eff, ash}}} \left[\frac{mol_{char}}{s, m^2_{part}} \right] \quad (66)$$

As the mechanical stress on the char particles in a fluidized bed is very large the outer ash layer is likely to be continuously removed and this resistance can therefore be neglected [6]. The other two resistances are however important. For calculation of the outer mass transport resistance, see 3.4.

The most important char reaction in an oxygen containing atmosphere is the oxidation reaction producing CO and CO₂. The ratio CO/CO₂ produced from the combustion can be calculated, according to Laurendal, by eq. (67) [69].

$$\frac{[CO]}{[CO_2]} = 2500 \exp\left(-\frac{52000}{RT}\right) \quad (67)$$

Kinetics for various chars with different coal origins, with the assumption of reaction only at the surface of the char is presented in Table 7, for the kinetic expression in eq. (68) [68].

$$k_{char\ kin.} = A_r T \exp\left(\frac{E_r}{RT}\right) \quad [m/s] \quad (68)$$

Table 7, kinetic parameters for various coals for the oxidation reaction between char and oxygen; $C + 1/2O_2 \rightarrow CO$

Coal	A _r [m/sK]	E _r /R [1/K]
High volatile bituminous coal A	1.03	9 010
High volatile bituminous coal C	0.50	6 310
Sub bituminous coal	10.4	11 200
Lignite	1.22	10 300

“Average coal”	2.30	11 100
----------------	------	--------

Other char reactions are much slower, but can be of some importance if the oxygen concentration is very low [68]. The main reactions are the reaction with hydrogen, the reaction with carbon dioxide and the reaction with water. The kinetics for the reaction with carbon dioxide is presented in Table 8, for the kinetic expression in eq. (68) [68].

Table 8, kinetic parameters for various coals for the reaction between char and carbon dioxide; $C + CO_2 \rightarrow 2CO$

Coal	A_r [m/sK]	E_r/R [1/K]
High volatile bituminous coal A	1 160	31 200
High volatile bituminous coal C	4 890	31 300
Subbituminous coal	6 190	28 900
Lignite	3.42	15 600
“Average coal”	589	26 800

According to Hobbs et al. the activation energy and pre exponential factor for the char reaction with water can be estimated as $E_{H_2O} = E_{CO_2}$ and $A_{H_2O} = A_{CO_2}$ while for the reaction with hydrogen the pre exponential factor is estimated to be three orders of magnitude smaller than the reaction with carbon dioxide, $A_{H_2} = 10^{-3}A_{CO_2}$, while the activation energy is estimated to be the same, $E_{H_2} = E_{CO_2}$ [68].

Adanez et al. investigated the reactivity of wood-chars in fluidized bed combustion [70]. Using a similar expression for the reaction rate as in eq. (66) and the same expression for the rate constant as in eq. (68) the values presented in Table 9 were found. Only the oxidation reaction with oxygen was considered.

Table 9, kinetic parameters for various wood types for the oxidation reaction between char and oxygen; $C + O_2 \rightarrow CO_2$. It can be noted that the variation between various wood-chars are relatively small [70].

Wood-type	A_r [m/sK]	E_r [kJ/mol]
Pine	1.23	70
Oak	1.06	68
Eucalyptus	1.05	71
Almond shell	0.95	71
Olive stone	1.12	67

During combustion the properties of the char particle will change. The two most popular models describing this change of the char particle is the un-reacting core model and the reacting core model [69]. The un-reacting core model is the simplest model, all reactions are assumed to occur at the surface of the particle, giving a decreasing diameter of the particle as it is consumed. This model is appropriate for large particle diameters and high temperatures, making the outer mass transport resistance dominating. The reacting core model uses the assumption that the reaction is homogeneously occurring throughout the particle, decreasing

the particles density. This model is appropriate to use at low temperatures and small particle diameters [69].

4. Method

A model of a bubbling fluidized bed is created. To decrease the computational cost, only very simple fluid-dynamics is used, mixed ideal tanks and mixed ideal tanks in series. Important behaviors are captured through the use of correlations.

The model is built to function with already existing models in Solvina's database.

When the model is completed it is verified through comparison with experimental data from an existing bubbling fluidized bed boiler and individual properties of the boiler are validated through comparison with existing values in literature.

4.1. Modeling the bubbling fluidized bed

The modeling of the bubbling fluidized bed combustion boiler is divided into two main areas, the bubbling fluidized bed and the freeboard.

4.1.1. The bed

Each of the phases in the system is modeled as a completely mixed ideal tank reactor to decrease the computational cost of the model. For the inert solid phase and the char phase this is likely a good assumption. Due to the short residence time of the gas in the bed, it may however be more accurate to model that as a plug flow, but this is too computationally costly. The bubbles in the bed move in a plug-like manner but are not modeled explicitly as this would require real kinetics for all phases, see section 4.1.1.4. Even though the bubbles are not modeled explicitly they are included in many correlations.

By not modeling the bubble phase explicitly all oxygen is available for the chemical reactions in the bed. In some cases this may be a very poor assumption and therefore the part of the oxygen bypassing in bubbles will be estimated, see section 4.1.1.5.

The drying and devolatilization are not modeled using kinetics, see section 4.1.1.4, therefore the only fuel phase in the bed is char.

No attempt is made to model the attrition of the char particles.

From the above assumptions three different phases exist in the bed. These are the inert solid phase, the gas phase and the char phase. The gas phase consists of a number of different species, see section 3.6. As equilibrium is assumed for methane, hydrogen and tar, these do not need a dynamic material balance. All char reactions are assumed to occur in the char phase while all gas phase reactions are assumed to occur in the gas phase. A material balance for species i is set up, see eq. (69). Index j stand for all homogeneous reactions and index k for all heterogeneous reactions.

$$\frac{dm_i}{dt} = m_{in,i} - m_{out,i} + \sum v_{i,j} r_j M_i V_{gas} + \sum v_{i,k} r_k M_i \quad (69)$$

An overall heat balance for the gas phase is also set up, see eq. (70). In this equation there is a transport of heat into and out of the bed. Heat is transferred between the bed and the char phase, as well as between the gas and the inert solids phase. The bed is cooled through both

water tubed walls and an immersed heat exchanger. The heat balance also includes a heat exchange term with the freeboard, see section 4.1.2.1.

As the heat transfer between the gas and inert solid phase is very large, with very low temperature differences, all heat transfer coefficients to the bed are considered to be allocated to the gas phase. If the temperature difference between the gas and inert solid phase turn out to be significant, this must be changed.

$$\begin{aligned} \rho_g C_{P,g} V_g \frac{dT_g}{dt} = & H_{in} - H_{out} + A_s N_s h_{g-s} (T_g - T_s) + A_c N_c h_{bed-c} (T_g - T_c) \\ & + A_{wall} h_{bed-w} (T_w - T_g) + A_{HX} h_{bed-HX} (T_{HX} - T_g) + \sum r_j \Delta H_{r_j} V_g \\ & + Q_{freeboard} \end{aligned} \quad (70)$$

A char phase mass balance is presented in eq. (71). There is no outflow of char as no char is assumed to leave the bed and the mass transfer therefore includes only an inlet flow and a consumption term.

$$\frac{dm_{char}}{dt} = m_{in,char} + \sum r_k M_{char} \quad (71)$$

The char phase heat balance is presented in eq. (72).

$$m_{char} C_{P,c} \frac{dT_c}{dt} = \sum r_k \Delta H_{r,k} + A_c N_c h_{bed-c} (T_g - T_c) + H_{in} \quad (72)$$

The inert solids phase does not need a mass balance as no mass is transferred to or from it. If attrition or the ash content of the fuel would be taken into account this would be needed as well. The heat balance of the inert solids phase is presented in eq. (73).

$$m_s C_{P,s} \frac{dT_s}{dt} = A_s N_s h_{g-s} (T_g - T_s) \quad (73)$$

The pressure drop over the bed is set equal to the weight of the bed, see eq. (3).

There are a number of unknowns in eqs. (69) to (73), the calculations of these unknowns are presented in sections 4.1.1.1 to 4.1.1.4.

4.1.1.1. Hydrodynamics

The hydrodynamics are needed in order to set limits for the minimum and maximum gas velocity, to calculate the gas volume, the height of the bed and the cooling area of the water tubed walls. Several of these properties are calculated using equations presented in section 3.2.1.

The minimum fluidization velocity is calculated using eq. (5), together with an estimate of the porosity at minimum fluidization by eq. (4), the real porosity can be calculated using eq. (7). With the real porosity and the volume and density of the inert material, the gas volume, bed height and wall area can be calculated easily.

The maximum fluidization velocity is calculated using eq. (6) and is used to control that the bed operates in the bubbling fluidized bed regime.

4.1.1.2. Heat transfer

There are four unknown heat transfer coefficients in the heat balances, these are the bed-char heat transfer, gas-inert solid heat transfer, water tubed walls-bed heat transfer and the immersed heat exchanger-bed heat transfer coefficient. These are calculated from equations presented in section 3.3.

The bed-char heat transfer coefficient is calculated using eq. (19), assuming the fluidization velocity is close to optimum. The gas-solid heat transfer coefficient is calculated using eq. (18) and the heat transfer coefficient between the bed and the immersed surfaces are calculated according to the procedure presented in section 3.3.3.

4.1.1.3. Mass transfer

The char kinetics presented in Table 7, Table 8 and Table 9 in section 3.6.6 are used depending on the type of fuel. These kinetics are based on the outer surface area of the particle, therefore no inner mass transfer is calculated. The outer mass transfer is calculated according to eq. (40).

4.1.1.4. Kinetics

As processes with fast time constants lead to a badly scaled system (very different time scales on kinetics and step size) and numerical instabilities during modeling the reaction kinetics are evaluated for possible simplifications, see Appendix I. Results show that very fast kinetics can be modeled as instantaneous, making the model faster and more robust. From simulations shown in Appendix I it is concluded that all kinetics except for the oxidation of carbon monoxide can be modeled as instantaneous. The kinetics for carbon monoxide oxidation is found in section 3.6.3.

The heterogeneous char reactions are significantly slower and need to be modeled, this is done using the kinetics in eqs. (66) to (68) together with the pre exponential factors and activation energies presented in Table 7, Table 8 and Table 9, all found in section 3.6.6.

The correlation for nitrogen oxide emissions presented in eq. (57) is shown to give a wrong behavior when compared to experimental data presented in literature, see Appendix III. Therefore a new simple correlation is done using experimental data presented by Oka [6]. The correlation is shown in Appendix III. An extensive simulation of the emissions of nitrogen oxides are also conducted using the kinetics from Table 6. These simulations are shown in Appendix III as well.

Sulfur retention is modeled using the procedure and equations presented in section 3.6.5.

The process of devolatilization is not dynamically modeled using kinetics as this is considered too computationally costly. Instead a time lag is introduced using a first order transfer function imitating the transient behavior of the real devolatilization. The time constant of the transfer function is set using eq. (55) in section 3.6.2. In other works the devolatilization has

been seen as instantaneous or modeled explicitly. A first order transfer function has a shape similar to the release of volatiles from devolatilization [6].

4.1.1.5. Bubbles

The largest effect the bubbles have on the combustion in the bed is that some of the oxygen in the bubbles is unavailable for combustion. To estimate the portion of the oxygen in the bubbles that would bypass combustion in the bed, an unsteady balance of a bubble moving through the bed is used, see eq. (74). For simplification the bubble size and velocity is assumed constant and equal to the bed average.

$$\frac{dC_b}{dt} = -K_{b-e}(C_b - C_e) \quad (74)$$

Solving the balance yields eq. (79).

$$C_{b,outlet} = C_e + (C_{b,inlet} - C_e)e^{(-K_{b-e}\tau_b)} \quad (75)$$

Using the volume fraction of the emulsion phase and the bubble phase and the velocity of both phases, the fraction of the oxygen not available for combustion can be estimated.

These calculations are made under the assumption that the limitations lie in the transport of oxygen from the bubbles to the emulsion phase and not in the transport of combustibles from the emulsion phase to the bubble phase.

Due to instabilities during simulation the oxygen bypass is not included in the final model, but can instead be added to the model using pure scaling factors. A small bypass is always activated in the model for stability reasons.

4.1.2. The freeboard

The freeboard consists solely of a gas phase. Particles hurled into the freeboard are not included in the model. Gas phase reactions can still occur so carbon monoxide oxidation is included. However, all other combustibles are already consumed due to the earlier assumption of instantaneous reactions. The gas in the freeboard move in a plug-like manner so approximation with a tank is not correct. The freeboard is instead approximated with a tank-series, to imitate the plug flow while not being as computationally demanding. The mass balance for each tank is similar to eq. (69).

The heat balance for a tank is shown in eq. (76). The heat balance contains radiative heat exchange with the bed, walls and the other gaseous volumes. There is also a convective heat transfer between the gas and walls. For better accuracy the mean temperature between the outlet and inlet of the tank is used in the radiation and convection terms. A tank series with six tanks are deemed accurate enough for a good prediction of the temperature profile in the freeboard, see Appendix II. Axial radiation is included in the model even though the effect is relatively low, as the computational cost is negligible.

$$\rho_g C_{P,g} V_g \frac{dT_g}{dt} = H_{in} - H_{out} + h_{conv} A_{wall} (T_w - T_{g,mean}) + Q_{rad-wall} + Q_{rad-bed} + Q_{rad,axial\ gas} \quad (76)$$

There is assumed to be no pressure loss in the freeboard.

The $Q_{rad,axial\ gas}$ is calculated using eq. (34) and $Q_{rad-wall}$ is calculated using eq. (38) found in section 3.3.4. For the bed radiation no appropriate model has been found. Therefore a model for the bed radiation is developed using a similar method as for the axial radiation presented in section 3.3.4.

4.1.2.1. Bed radiation

The bed radiation is modeled in a similar manner to the axial gas to gas radiation. Radiative heat from the bed first comes in contact with the gas in the first tank. The fraction absorbed equals the gas emissivity (assuming the emissivity equals the absorptivity). Calculation of a view factor for the top of the gas volume yields an estimate for the amount of radiation continuing to next gas volume. The fraction of radiation not absorbed in the gas and not continuing to the next gas volume is radiated to the walls, see Figure 6. Equations for the amount of radiative heat exchanged between the bed and gas and between the bed and walls are given in eq. (77) and eq. (78).

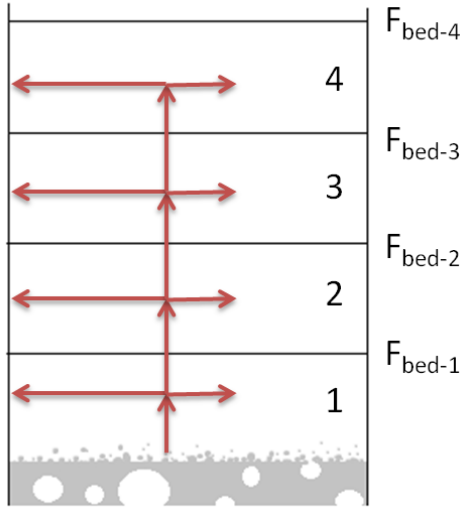


Figure 6, schematic figure of how part of the gas radiation is absorbed to the gas and walls of each tank. The view factors, F_{bed-i} , are calculated according a set of equations presented in [71].

$$Q_{rad-bed} = \varepsilon_{g,i} \left(\prod_{k=1}^{i-1} (1 - \varepsilon_{g,k}) \right) F_{bed-(i-1)} E_{Bed,net} \quad (77)$$

$$Q_{rad-wall} = \varepsilon_{wall} \left(\prod_{k=1}^i (1 - \varepsilon_{g,k}) \right) (F_{bed-(i-1)} - F_{bed-i}) E_{Bed,net} \quad (78)$$

The sight factors in eq. (77) and eq. (78) are calculated according to the equation for rectangular or circular parallel plates depending on geometry [71]. $E_{Bed,net}$ is the net radiative

heat exchange between two surfaces situated directly next to each other. It is calculated similarly to eq. (38), see eq. (79).

$$E_{bed-gas/wall} = \frac{A_{gas/wall} \sigma (T_{bed}^4 - T_{gas/wall}^4)}{\frac{1}{\varepsilon_{bed}} + \frac{1}{\varepsilon_{gas/wall}} - 1} \quad (79)$$

5. Simulation of the boiler model

The boiler model is evaluated by studying its transient and steady state behavior and studying important properties of the boiler. The individual objects in Dymola have been evaluated separately by estimating if the behavior is reasonable and by checking material and energy balances. Many areas have been simulated and evaluated using Matlab before being implemented into the main code in Dymola. Some of these areas are shown in appendices, but in this chapter only simulations based on the final model are presented.

Due to the very large amount of parameters in the model, variation of all of the parameters cannot be shown, but only the most important and influential are presented. The dimensions and boiler properties are set using data from an existing 16 MW_{th} bubbling fluidized bed boiler at Chalmers presented by Johnsson et al. [72]. The properties of the boiler are presented in Table 10.

Table 10, properties of the 16MW_{th} boiler presented in [72].

16 MW _{th} bubbling fluidized bed boiler at Chalmers	
Bed cross section	3.4 m×2.9 m
Height of the unit	5.7 m
Bed material	Silica sand and coal ash
Bed material density	2600 kg/m ³
Average particle diameter	0.56 mm
Fixed bed height	0.75 m
Bed temperature	1070-1170 K
Superficial gas velocity	1.2-2.3 m/s
Minimum fluidization velocity	0.12 m/s

The most interesting parameters to investigate are the air to fuel ratio and the boiler load. Interesting outlet properties is the outlet concentrations of carbon monoxide, nitrogen oxide and sulfur dioxide, the temperature of the bed and along the freeboard and the total heat uptake of the modeled part of the boiler. The char content in the bed are also presented as this can have a significant effect during transients.

Individual properties of the boiler model are evaluated from experimental data found from literature. These properties include the temperature levels and heat transfer of different parts of the boiler, the char loading in the bed and the emission of sulfur dioxide and nitrogen oxide from the boiler.

Finally the model is adapted to follow the behavior of a real bubbling fluidized bed boiler, Riskullaverket owned by Mölndal Energi.

5.1. Varying the air to fuel ratio

The first test on the model is variation of the air to fuel ratio. This is done using a high volatile coal as fuel with a water content of 10%. The air inlet temperature is 195°C, the air flow is 3.8 kg/s and the fuel input is 0.33±0.11 kg/s. This yields an air to fuel ratio of 1.15, 0.87 and 1.73. The temperature of the bed solid phase, gas phase, char phase and each freeboard slice is

presented in Figure 7a. Figure 7b-d show the temperature profile over the furnace for the three steady state cases.

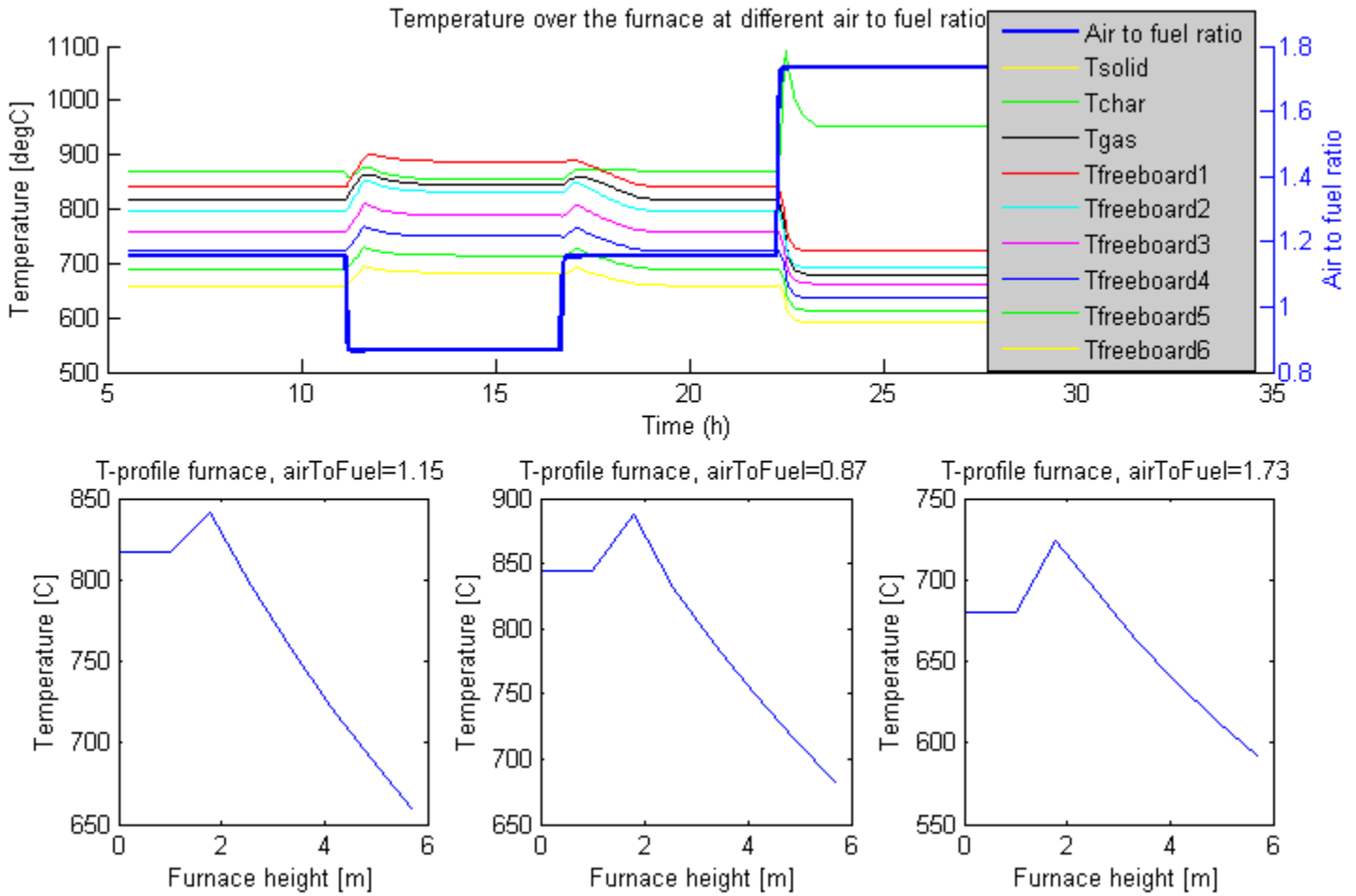


Figure 7a, the transient behavior of the temperature in each part of the boiler when changing the inflow of fuel so that the air to fuel ratio varies between 0.87 and 1.73. Figure 7b-c, steady state temperature profile over the boiler for each of the air to fuel ratios.

When decreasing the air to fuel ratio (increasing fuel input) the temperature over the bed and freeboard rise according to Figure 7a. This is expected as more fuel is combusted for the same air flow, thus releasing more energy into the flow. It is also notable that the temperature difference between the bed and char decreases as the air to fuel ratio is decreased. This is due to the lower oxygen concentration in the bed yielding a slower char combustion per char particle and thereby a smaller heat evolution compared to the heat transport from the char particle to the bed.

Decreasing the fuel input to the earlier level temporarily lead to an increase in bed and freeboard temperature before stabilizing at earlier temperatures. Due to the sudden increase of oxygen in the bed, more char combustion can occur, temporarily raising the bed temperature until a steady state char loading is achieved.

Decreasing the fuel input so that an air to fuel ratio of 1.73 is achieved lead to significantly lower temperatures for the bed and freeboard. This is also expected as the heat evolution is lower with lower fuel inputs. The decrease in fuel input lead however to a significant rise in char temperature. As the fuel input is decreased more oxygen is available for the char combustion, leading to very fast char combustion. The fast combustion leads to higher heat evolution and thereby higher char temperatures.

From Figure 7b-d the temperature increase significantly at the start of the freeboard before decreasing close to linearly. This increase is due to the oxygen and carbon monoxide bypass induced in the bed for stability reasons. As this bypass usually occurs in real beds due to the bubbles this temperature profile resemble real beds more closely than without the bypass (at least for high volatile fuels). At high overall temperatures the temperature drop over the freeboard is larger (Figure 7c) compared to the case of lower overall temperatures (Figure 7d). This is expected as higher temperature differences lead to higher heat transfer.

Figure 8a below show the effect of air to fuel ratio on carbon monoxide concentration, while Figure 8b show the char content in the bed and Figure 8c show how the emissions of nitrogen oxide and sulfur dioxide.

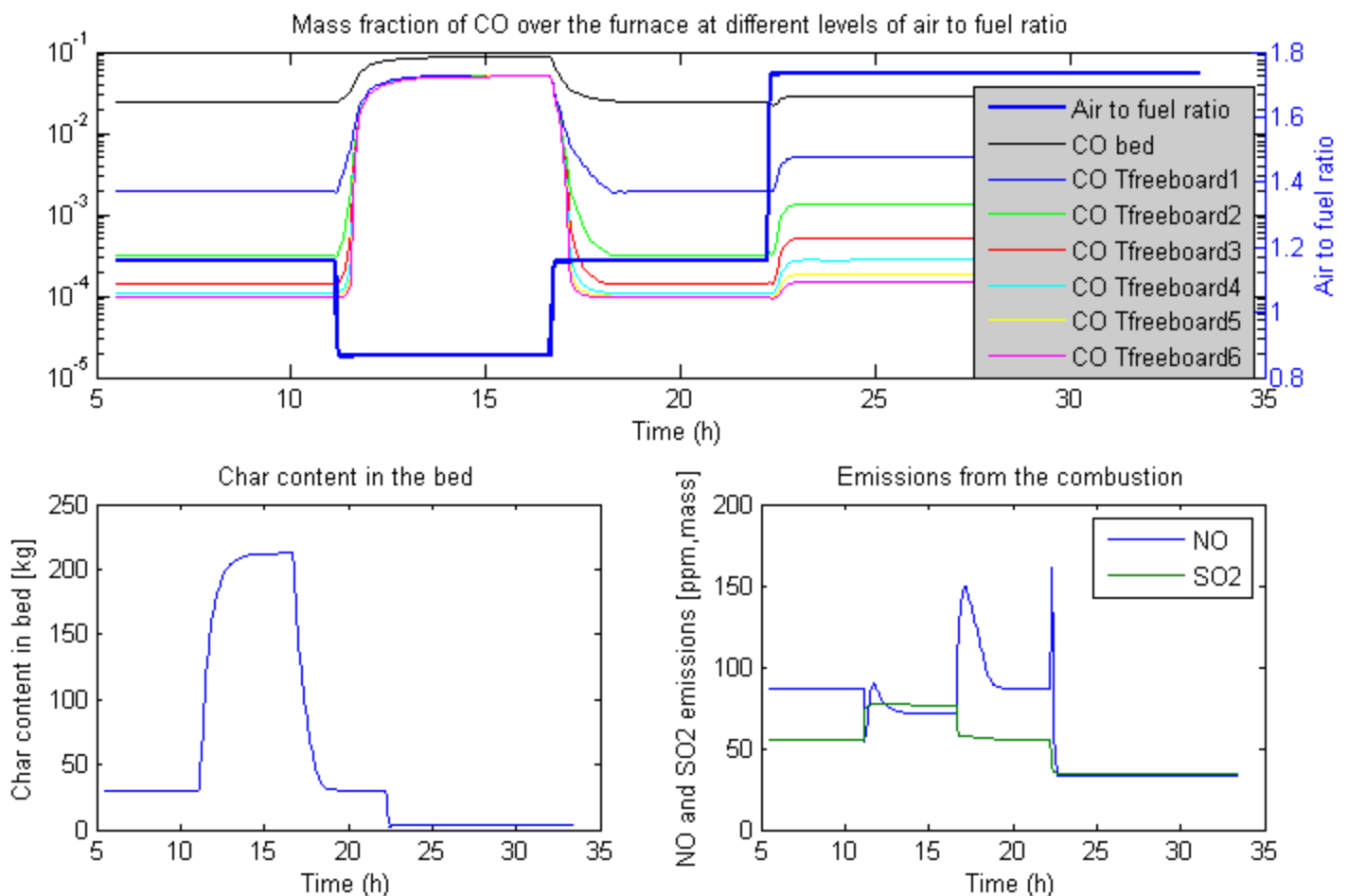


Figure 8a, the transient behavior of the carbon monoxide mass fraction in each part of the boiler when changing the inflow of fuel so that the air to fuel ratio varies between 0.87 to 1.73. Figure 8b, mass of char in the bed. Figure 8c, levels of nitrogen oxide and sulfur dioxide in mass ppm.

According to Figure 8a, the mass fraction of carbon monoxide increases sharply as the air to fuel ratio drop below one, as there is not enough oxygen available for complete combustion. When decreasing the fuel input below normal levels the carbon monoxide concentration seem to first drop somewhat, before increasing to levels above those before the decreased fuel input. The first decrease in carbon monoxide concentration is likely due to a higher concentration of oxygen. When the bed has cooled off this effect is counteracted by the overall lower temperature yielding slower carbon monoxide oxidation.

The char loading in the bed increase sharply as the air to fuel ratio drop below one according to Figure 8b. At an air to fuel ratio at 1.73 the char loading seem to decrease sharply to very low levels. These changes occur due to the changing availability of oxygen in the bed.

In Figure 8c, the emissions of nitrogen oxides changes rapidly when changing the air to fuel ratio. When the air to fuel ratio is decreased the nitrogen oxide emissions drop rapidly before increasing again and stabilizing at a slightly lower level than before. The rapid drop is due to the fast decrease in oxygen availability while the increase is due to a higher bed temperature. By increasing the fuel to air ratio again the emissions rapidly increase, as the oxygen availability increase sharply while the bed temperature still is high. When the bed temperature drops the emission levels decrease again. The same behavior is seen when the air to fuel ratio is increased further. Due to the very low bed temperature the emission levels at steady state are very low with the highest air to fuel ratio.

It should be noted that these transient behaviors of the nitrogen oxide emissions likely are exaggerated as the emission levels are correlated against the air to fuel ratio, see Appendix III. Correlation against the bed oxygen concentration would however remove the transients all together as the char content in the bed will consume the extra oxygen during an increase in air to fuel ratio. For absolutely correct transient behavior, an extensive kinetic model for the nitrogen oxide emissions is needed where char and nitrogen compete for the oxygen. However, for the real time simulator application, the very much simplified nitrogen oxide model presented in Appendix III has been found sufficient.

The emission levels of sulfur dioxide follow the input of fuel, with higher sulfur dioxide emissions with more fuel (and thereby sulfur) input. The emission levels show no transient behaviors.

The superficial gas velocity in the bed varies somewhat, from about 1.3 m/s at the normal conditions, up to 1.4 for the low air to fuel ratio and then down to 1.1 m/s at the high air to fuel ratio.

5.2. Varying the boiler load

The next test is to vary the load of the boiler. This is done with a constant air to fuel ratio of 1.15. The fuel input is 0.33 ± 0.11 kg/s while the inlet air flow is 3.8 ± 1.267 kg/s. The temperatures of the bed solid phase, gas phase, char phase and each freeboard slice are presented in Figure 9. Figure 9b-d show the temperature profile over the boiler for the three steady state cases.

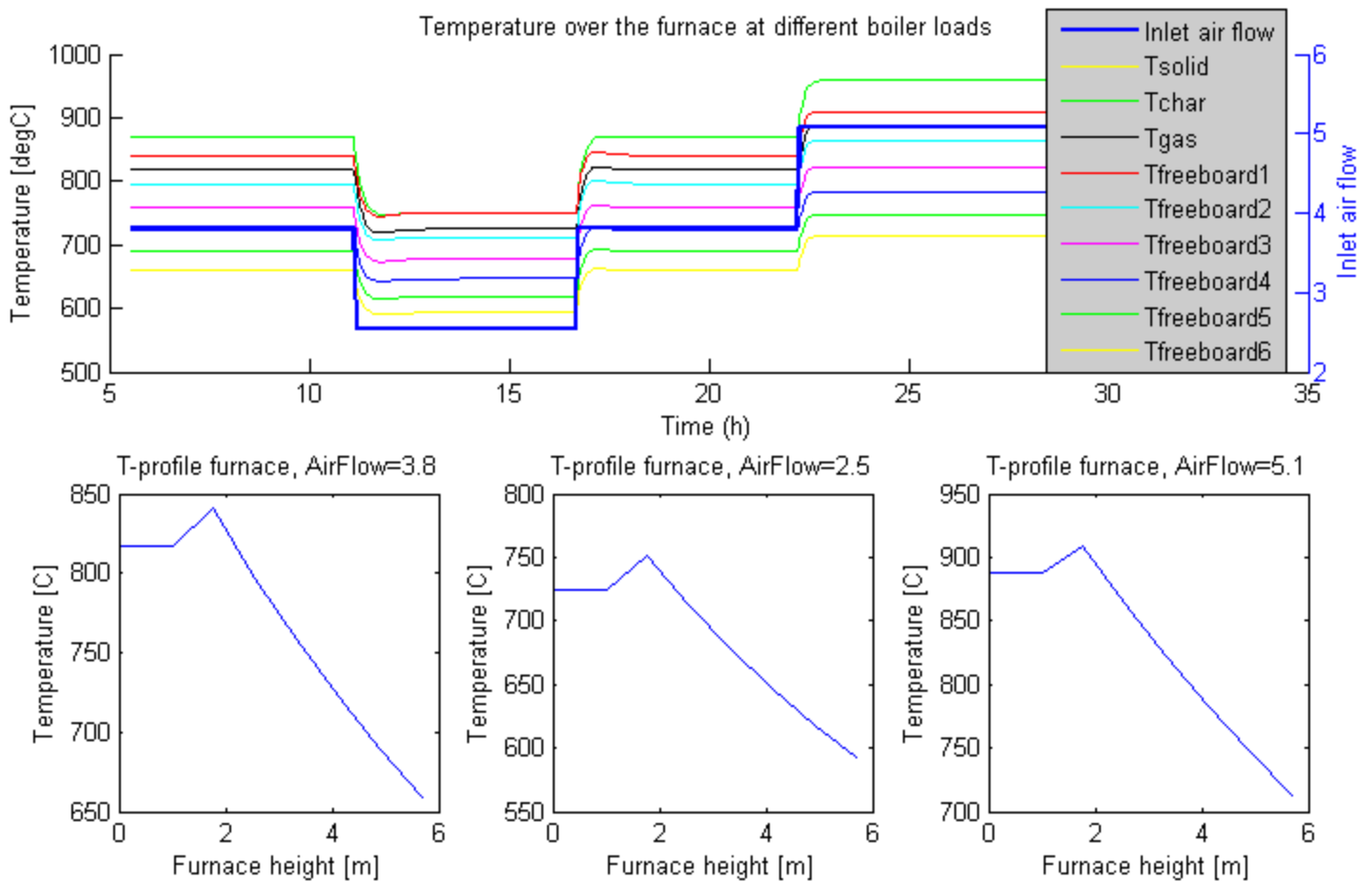


Figure 9a, the transient behavior of the temperature in each part of the boiler when changing the load of the boiler. Figure 9b-c, the steady state temperature profile over the boiler for each of the boiler loads.

According to Figure 9a, the temperature profile of the boiler follow the load, with decreased temperatures at lower loads and increased temperatures at higher loads. The temperature profiles of the boiler are similar to those shown in Figure 7b-c, with increasing temperature at the beginning of the freeboard and then close to linearly decreasing temperatures.

Figure 10a show the effect of boiler load on carbon monoxide concentration, while Figure 10b show the char content in the bed and Figure 10c show how the emissions of nitrogen oxide and sulfur dioxide at varying boiler load.

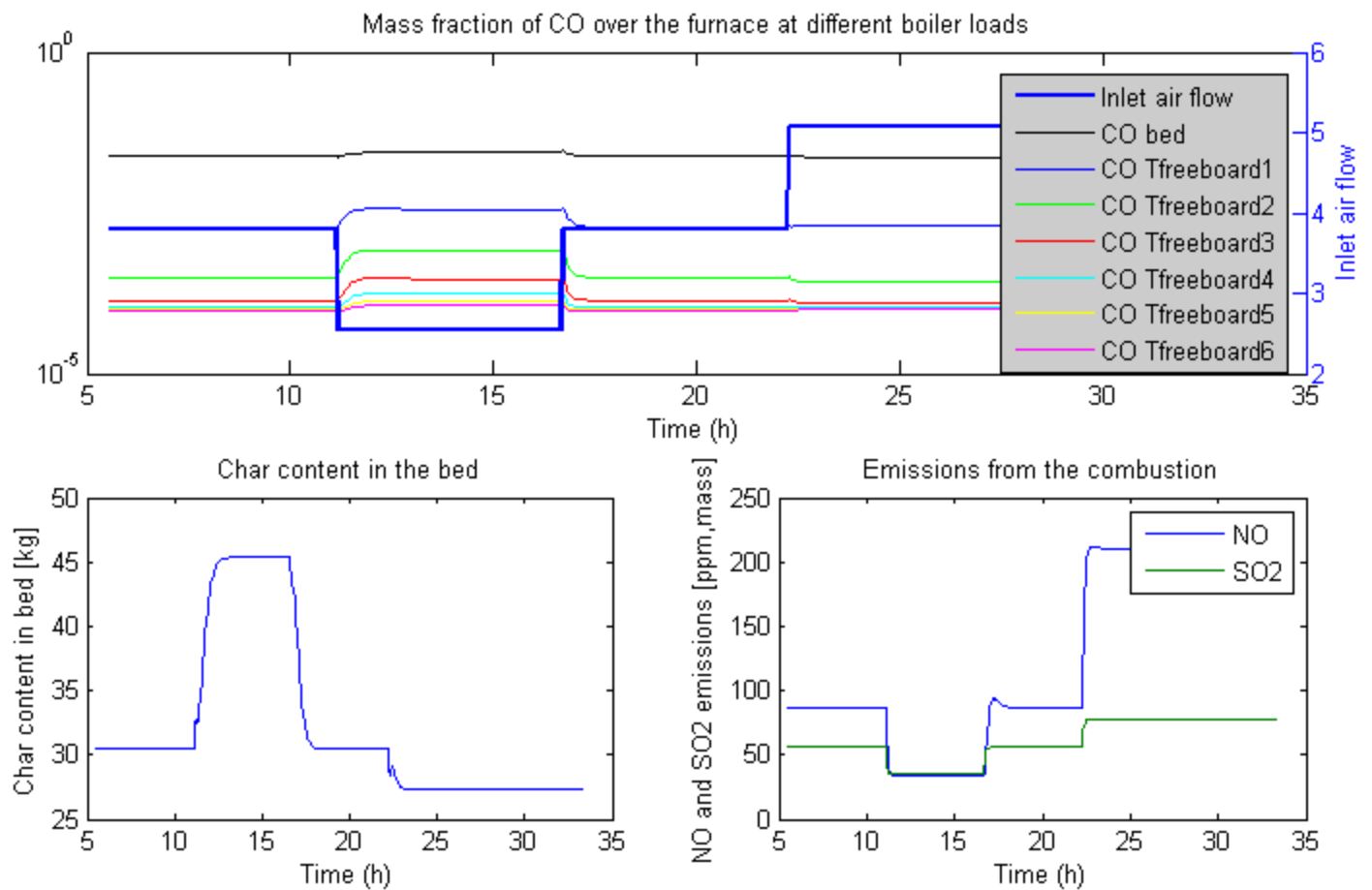


Figure 10, the transient behavior of the carbon monoxide mass fraction in each part of the boiler when varying the boiler load. Figure 10b, mass of char in the bed. Figure 10c, levels of nitrogen oxide and sulfur dioxide in mass ppm.

According to the simulation in Figure 10a the carbon monoxide emission levels increase with the lower boiler load. This is logical as the temperature drop significantly at this low boiler load and thereby the carbon monoxide oxidation rate. Other carbon monoxide transients when changing the load is however small.

In Figure 10b the mass of char in the bed increase somewhat when decreasing the boiler load. This is also due to the lower bed temperature, making char oxidation slower.

The emission levels of both sulfur dioxide and nitrogen oxide decrease with lower boiler load and increase with higher boiler load. The nitrogen oxide emissions are highly temperature dependent and therefore more than double at the high boiler load, with the higher bed temperature, compared to the initial boiler load. The sulfur dioxide emissions follow the fuel input, with higher emission at high fuel input. As the lime residence time get lower for higher boiler loads (higher input for the same bed size yield shorter residence time) this likely effect the emissions as well.

The superficial gas velocity in the bed varies with load, ranging from about 1.3 m/s at the normal conditions, up to 1.9 m/s for the high boiler load and down to 0.8 m/s at the low boiler load.

5.3. Verification of temperatures and heat transfer

From the book by Oka the temperature difference between the bed and gas is seldom more than a few degrees [6]. From the simulations shown in Figure 7a and Figure 9a, the temperature profile of the solid phase cannot be seen as it is covered by the temperature profile of the gas phase. So the temperature difference between the solid phase and the gas phase in the bed is very low.

According to Oka the char temperature is typically 50-250°C above the temperature of the bed [6]. From the simulation shown in Figure 7a, it is clear that the temperature difference varies a lot depending on the air to fuel ratio. At the initial air to fuel ratio the temperature difference is about 60°C, decreasing to 20°C when the air to fuel ratio is 0.87 and increasing to 260°C when the air to fuel ratio is 1.73. Due to the large changes in temperature difference between the bed and char it is hard to validate. The overall behavior of the model is however correct. Boiler operation with a low air to fuel ratio means a slower char combustion and heat evolution and thereby a low temperature difference between the phases, as the simulations show.

According to experimental values presented by Biyikli et al. the heat transfer coefficient varies between 120-140 W/m²K in the freeboard region for fluidization velocities of 1-2 m/s and a bed temperature of 750°C [73]. Oka presents a heat transfer model and experimental values from Andersson et al. for a bubbling fluidized bed boiler at Chalmers [6]. According to the experiments the heat transfer coefficients are around 100 W/m²K, somewhat higher close to the bed and lower higher up in the furnace.

From various experimental results presented by Oka, the heat transfer coefficient between the wall and immersed surfaces should lie in the range of about 300-500 W/m²K for the particle size used in the current set up (0.56 mm) [6].

Figure 11 below show the heat uptake and the estimated heat transfer coefficient along the furnace for the high boiler load simulations case shown in Figure 8 and Figure 10. The wall temperature is set to 400°C. The heat transfer coefficient is estimated for each part of the boiler by using the heat transferred to the specific wall section together with the area and temperature difference in the specific part. This means that the heat transfer coefficients in the freeboard slices contain both convective and radiative heat transfer from the gas as well as the bed radiation to the specific section.

A weighted average of the heat transfer coefficients shown in Figure 11 for the freeboard yields an average heat transfer coefficient of 98 W/m²K. This is close to the values found by Oka and by Biyikli. The heat transfer coefficient in the bed in the model is around 480 W/m²K according to Figure 11. The bed heat transfer coefficient is thereby in the interval described by Oka. For higher loads the heat transfer coefficients are slightly higher and for lower loads the heat transfer coefficients are somewhat lower in the simulation model.

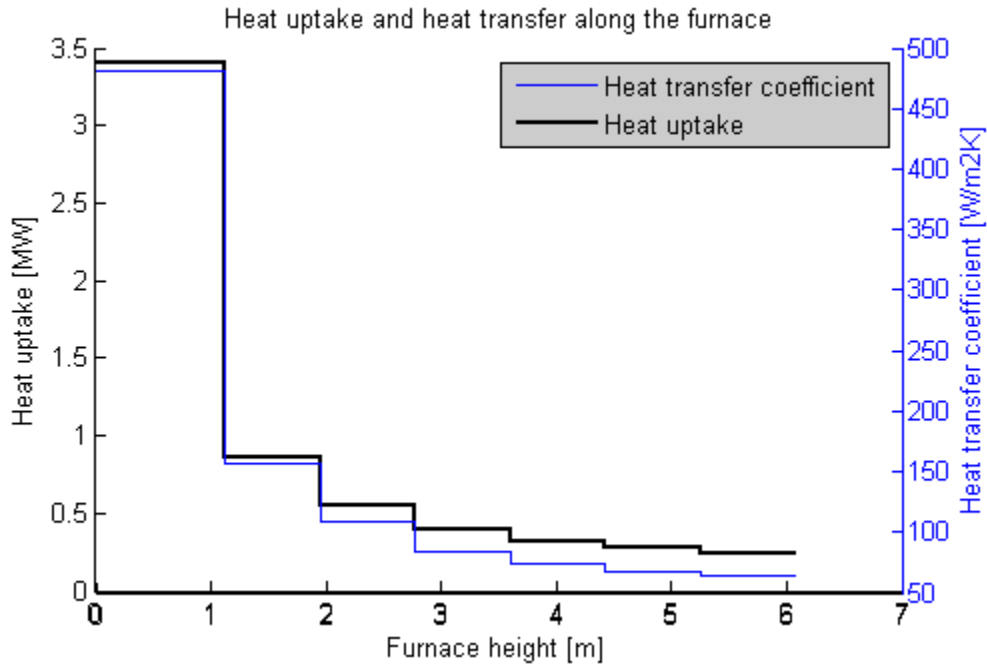


Figure 11, the total heat transferred to the walls of each boiler section and the heat transfer coefficients in each section for the normal operation case.

5.4. Verification of bed load and emissions

The char loading for combustion of coals are typically 2-5wt% of the bed [6]. The simulations showed in Figure 8c and Figure 10c show values ranging from about 0.1-2 wt% of the bed. The lower char content is probably a result of neglecting the bubble resistance to oxygen availability.

The emission of sulfur dioxide is mainly dependent on the lime to sulfur molar ratio in the inlet flow, the lime particle diameter and the reactivity of the lime according to Lin et al. [61] [59] [58]. Figure 12 show a simulation of the sulfur retention for 1 mm diameter lime particles at variable lime to sulfur molar ratio in the inlet with the created boiler model.

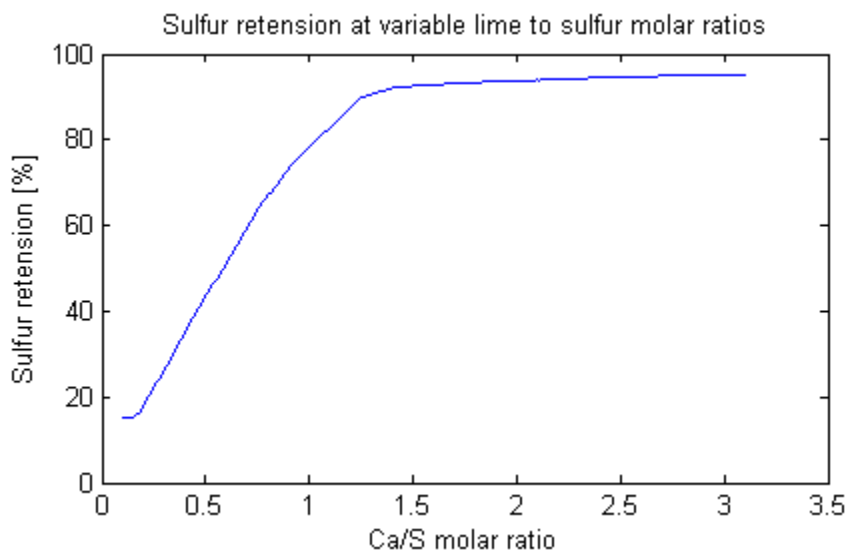


Figure 12, sulfur retention efficiency as a function of lime to sulfur molar ratio for lime particles of 1 mm using the created boiler model.

Experimental values for the sulfur retention vary a lot depending on boiler and operating conditions [6]. Experimental values from the bubbling fluidized bed at Chalmers presented by Oka show that the typical sulfur retention efficiency lie around 40-60 % for a lime to sulfur ratio of one [6]. From Figure 12 the sulfur retention is around 80 %. For very high lime to sulfur ratios the efficiency reaches 90 % for the boiler at Chalmers, while Figure 12 show values of about 95 % [6]. Boilers using fly ash recirculation have in general higher sulfur retention. A boiler presented by Oka with high fly ash recirculation and lime to sulfur molar ratio of 3.5 have a sulfur retention of above 96 % [6]. As no attrition or elutriation is considered in the boiler model, the simulation results are most comparable with experimental values from boilers using a high fly ash recirculation. The overall shape of the curve presented in Figure 12 is the same as those presented elsewhere [6].

The nitrogen oxide emissions from bubbling fluidized beds most often lie between 50 and 300 ppmv according to Oka. From the simulations presented in Figure 8 and Figure 10 the nitrogen oxide emissions varies between 40 and 250 ppmv.

The emission of nitrogen oxides increases with increasing air to fuel ratio and decreases with decreasing bed temperature. This is the correct behavior according to experimental values presented by Oka and by Chyang et al. [6] [74]. The absolute values shown during simulations are reasonable but may not be absolutely correct, see Appendix III.

5.5. Model comparison with existing boiler; the Riskulla CHP

Riskulla CHP is a new 70 MW bubbling fluidized bed boiler owned by Mölndal Energi. The unit is designed to burn biomass, mainly wood branches and wood tops. It uses ammonia injection to reduce the emission levels of nitrogen oxides. Wood branches and tops contain very low amounts of sulfur and sulfur retention is therefore not necessary. The efficiency of the boiler is very high due to usage of flue gas condensation.

The specifics of the boiler are presented in Table 11.

Table 11, the specifics given of the Riskulla CHP. The data has been given by Karl-Fredrik Karlsson at Mölndal Energi.

70 MW_{th} Riskulla bubbling fluidized bed boiler	
Bed cross section	6.8 m ² × 5.9 m
Height before super heater (total height)	15 m (30 m)
Bed material	Sand and biomass ash
Total bed weight	100 000 kg
Bed particle diameter	1 mm
Bed height during operation	0.50 m
Temperature primary air (secondary air)	196°C (199°C)
Bed temperature	830°C
Gas temperature before super heater	920°C
Air to fuel ratio	1.02
Total air flow	24.6 Nm ³ /s = 29.1 kg/s
Primary air flow	11.2 Nm ³ /s = 13.3 kg/s
Fuel usage 100% load (branches and tops)	85 m ³ /h
NO _x emissions (with ammonia injection)	60 mg/MJ
SO ₂ emissions (burning branches and tops)	0 mg/MJ

CO emissions	160 ppm
Water tubed walls	130 bar, 330°C
Outlet steam	130 bar, 520°C

Several aspects differ between this boiler and the boiler model. For instance this boiler uses fuel injection above the bed, causing a lot of the drying and devolatilization to occur above the bed instead of inside it. It uses a staged combustion with air injected above the bed at several locations. This causes much of the combustion to occur above the bed and not in it. The low height of the bed is also likely causing a large air bypass by bubbles and thereby low bed oxygen levels.

Although Mölndal Energi has been very helpful in providing data on the Riskulla CHP, some additional data have to be estimated. These are the average fuel particle size, the moisture content in the fuel and the nitrogen and sulfur content in the fuel. The fuel density also needs to be estimated.

The fuel density, 320 kg/m^3 , is given from [75]. Using this density together with the fuel flow given in Table 11 gives a total mass flow rate of fuel of 7.56 kg/s.

The fuel particles are likely to have a very wide size distribution, ranging from dust to small wood chips. A fuel particle size of 5 mm in diameter is deemed to be a good estimate and is used in the model. The water content in tops and branches depend on the freshness of the fuel. Fresh branches and tops typically contain 45-55 wt% moisture and stored typically 30-45 wt% moisture [75]. A moisture content of 43 wt% is set as this gives an accurate air to fuel ratio of 1.02 and is a reasonable mean value. The nitrogen content is set to 0.7 wt% and the sulfur content to 0.05 wt%, typical values for branches and tops in Sweden [76].

The wall temperature of the boiler is set to 330°C. The heat transfer coefficient from boiling water is significantly higher than the heat transfer coefficient on the flue gas side. This mean that the wall temperature will be close to the temperature of the boiling water and 330°C is thereby a good estimate.

To better predict the performance of the Riskulla boiler, a secondary air inlet is added to the model at three locations in the freeboard before the super heater, similarly to the air injection in the Riskulla boiler. From the data presented in Table 11 the boiler uses an extremely low primary air ratio of only 0.47. Due to assumptions made during the modeling, the air to fuel ratio of the model cannot be that low. The lowest air to fuel ratio possible to use in the model is 0.6, giving a primary air flow of 17.46 kg/s. The secondary air flow is 11.64 kg/s, divided equally over the three inlets in the freeboard.

Due to the significantly higher primary air to fuel ratio in the modeled bed compared to Riskulla and earlier modeling assumptions (see Appendix II), more heat is released into the bed. To recreate the values presented in Table 11 the heat uptake in the bed is increased by a factor three and the heat uptake in the freeboard is decreased by a factor 0.6. Using this scaled heat uptake the temperature and carbon monoxide concentration profile is found in Figure 13.

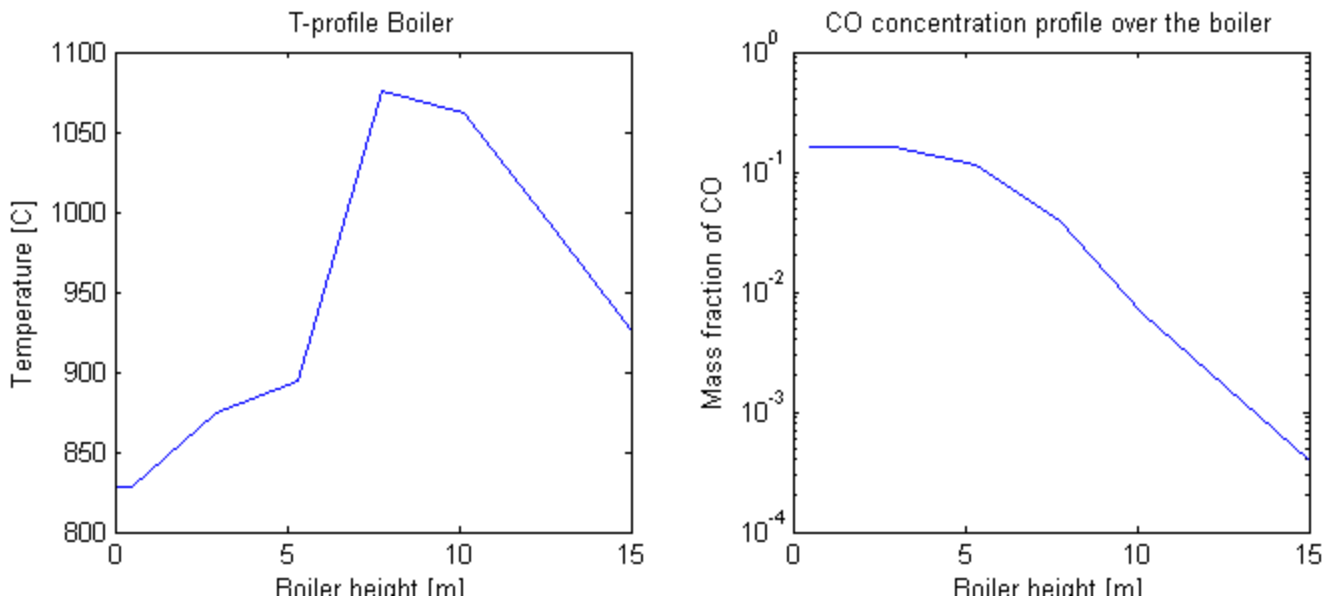


Figure 13a, the temperature profile along the furnace. Figure 13b, carbon monoxide concentration along furnace.

The temperature profile found in Figure 13a follow the temperatures given in Table 11, but as only two values along the furnace are given it is hard to validate the profile. It is however likely that the temperature continues to increase significantly in the freeboard as more air is added. When most of the carbon monoxide is oxidized the temperature should start to drop, as can be seen in Figure 13. The outlet carbon monoxide concentration before the super heater is about 400 ppm according to the model. This seem as a reasonable value as is should not drop to 160 ppm until the stack according to the values from the Riskulla boiler. As ammonia is injected into the furnace the emission levels differ significantly for the nitrogen oxides, these needs to be scaled also for accurate results. Also the emission of sulfur dioxide is not zero as the fuel is assumed to contain some sulfur.

6. Discussion

A number of aspects of the modeling of the boiler will be discussed. First the largest difficulties that occurred during the modeling will be thoroughly discussed and then the performance of the final model will be discussed and the possibility to adapt the model to an existing boiler.

6.1. Main difficulties during modeling

During modeling a number of difficulties occurred. These will be discussed more thoroughly. The largest difficulties during the modeling were the inability to use fast kinetics, the modeling of the emission levels of nitrogen oxide and sulfur dioxide, the bubble phase modeling and modeling of the radiation in the freeboard.

6.1.1. Fast kinetics

The usage of fast kinetics in combination with the much slower time constants in for example the mass transport, gives an ill-conditioned system with numerical problems. A combination of fast kinetics and too large time steps taken by the solver can also result in un-realistic states as resulted in a negative concentration of the specific substance. When the kinetics is very fast the time steps have to be extremely small to prevent the concentration of a reactant to be negative. Extremely small time steps, on the other hand gives a higher risk of slow simulations.

To handle the numerical problems and to get a more stable and faster model, fast kinetics is modeled as instantaneous. The combustion of carbon monoxide was kept as this is the most important combustible formed under air to fuel ratios below one. Other solutions to the numerical problems with fast reactions may exist but using instantaneous reactions was deemed to be a simple and stable solution.

From Appendix I it is clear that the methane formed during devolatilization does not always combust quickly. The methane was despite of this seen as instantaneous as the model was not expected to operate at very low air to fuel ratios (at which the assumption is appropriate). Usage of methane would also mean that the medium model used would have to be modified as methane is not a part of it.

6.1.2. Emission of nitrogen oxide

The emission of nitrogen oxide from the bed is a very complex process due to many competing reactions and their dependence on the type and amount of solids in the bed. The char content has a significant effect on the emission levels, as does the ash content and the type of solid phase. Many fuel dependent parameters are also important. An accurate modeling of the emissions is hard to accommodate.

Most existing models for nitrogen oxide emissions from bubbling fluidized beds use extensive reaction kinetics with a large number of reactions. Many of these reactions are very fast making implementation in Dymola hard. Empirical correlations for the nitrogen oxide emissions from fluidized bed boilers are rare and usually quite old. The three found correlations are from the 70s and 80s. None of the correlations have the same behavior as the experimental values found. One of the models have decreasing emissions with increasing air

to fuel ratio and one of them have decreasing emissions with increasing bed temperature [49] [50]. A new correlation is built based on experiments presented by Oka. This correlation has the behavior described in literature [6] [74]. The absolute values from this correlation may however not be entirely correct, especially at conditions outside the range at which the correlation is created.

6.1.3. Emission of sulfur dioxide

The emission of sulfur dioxide in a bubbling fluidized bed using limestone addition is a very complex process. The added limestone is calcinated, resulting in a porous calcium oxide particle. The sulfur dioxide reacts with the calcium oxide plugging the pores in the particle as the formed calcium sulfate has a significantly larger volume than calcium oxide. This makes further reaction slower and slower the more the pores are plugged. Due to pore plugging the calcium oxide in the center of the particle may be completely blocked from reaction. No model describing these steps in a computationally cheap way has been found and therefore a simpler model is used. The model is developed for a specific boiler and a specific type of limestone. The accuracy for other boilers and types of limestone is unknown.

The shown emission levels during simulation is relatively low, likely the sulfur retention is a bit too effective. To accurately predict the emissions from a specific boiler the emission levels have to be scaled. The behavior of the sulfur dioxide emissions during variable operating conditions are however reasonable.

6.1.4. Bubble phase

For accurate modeling of the bubble phase in the bed, the kinetics cannot be seen as instantaneous. Species transport between the phases has to be allowed for accurate predictions. As real kinetics cannot be used in the model, an estimate of the oxygen transfer from bubbles to emulsion phase can be calculated. This is under the assumption that it is the oxygen transfer from the bubble phase to the emulsion phase that limits the combustion and not the species transport from the emulsion to the bubble phase. Calculations show that this mass transfer between the phases is not always fast enough to make all oxygen available to the bed combustion. The accuracy of these calculations are however questionable and they are not included in the final model. A scaling factor is instead used so that some of the oxygen can be bypassed the bed if this is needed.

It should be noted that a model with real modeling of the bubble phase is likely to be too computationally costly to run at real time.

6.1.5. Radiation in the freeboard

The radiation in the freeboard area is relatively complex. Radiation comes from each gas volume in the tank series, from the walls and from the bed. If the freeboard area was modeled as a large mixed tank, modeling would have been easy, but this was deemed too simple and inexact. Several advanced models exist for calculation of radiative heat exchange between gas volumes, one of them is the zonal method. This modeling approach is however complex and computationally costly. A simple method developed by Bueters et al. and refined by Dounit et al. was used in the model [29] [30]. As can be seen in Appendix II, the gas to gas radiation does not have a significant effect on the final temperature profile.

The bed radiation has a significant effect on the freeboard temperature profile. No models were however found to model the bed to gas and bed to freeboard wall radiation. Therefore a model was developed based on the same principles as the gas to gas radiation model presented by Dounit et al [30]. The model is reasonable, looking at the temperature profiles in Appendix II. The temperature profiles including the bed radiation is more similar to experimental data than the models excluding bed radiation. The bed to wall radiation has a clear effect on the heat transfer coefficient in the freeboard as can be seen by the higher heat transfer coefficients in the beginning of the freeboard, see Figure 11.

6.2. Overall model performance

Despite several simplifications in the model, the overall performance of the model is satisfying. During simulations with variable boiler load and variable air to fuel ratio the model behaves logically. The model is able to capture transient behaviors and the transients are reasonable.

The verification of the different parts of the boiler shows that model predictions are similar to experimental values. The two uncertain parts of the boiler model are the emissions of nitrogen oxide and sulfur dioxide. These are highly dependent on the characteristics of the bed, limestone and char content and are therefore also hard to validate. Further improvements on the model should focus on these parts if they are of importance.

The model is adapted to an already existing boiler, a boiler that differs significantly in some aspects. The boiler has a significant air staging with a calculated primary air to fuel ratio of less than 0.5. The created model does not work with a primary air to fuel ratio of less than 0.6. At this low air to fuel ratio the assumption of instantaneous gas reactions is questionable. Due to the higher air to fuel ratio and errors arising from the low air to fuel ratio, the bed cooling had to be increased to get the same temperature as in the real boiler. The heat uptake in the freeboard area had to be decreased for the same reason. With this scaling, the temperature profile and carbon monoxide concentration throughout the boiler is reasonable and similar to the existing boiler. As the boiler also uses ammonia injection to reduce nitrogen oxide emissions, these had to be scaled accordingly.

7. Conclusions

A real time simulation model for bubbling fluidized bed combustion has been created. The model behaves logically during transients and steady state operation. If the model is used to mimic an already existing plant and these differ it is possible to adapt the model using scaling variables on major outputs and parameters.

Due to stability problems using real kinetics only a few reactions were modeled kinetically. Most of the reactions are seen as instantaneous or estimated using correlations. The bubble phase was not modeled explicitly, but the influence of the bubble phase has been added using simple scaling variables. By not modeling the bubble phase explicitly the model loses accuracy for prediction. There has been an extensive use of correlations in the model which is a good and computationally cheap way of getting a realistic behavior.

The largest difficulties have been to predict the emissions of sulfur dioxide and nitrogen oxide as the kinetics is fast and thereby couldn't be used as this would lead to large instabilities. The sulfur dioxide emissions are modeled using a simple model giving the correct behavior but the absolute values of the emissions are somewhat underrated. The simple correlations found in literature for the nitrogen oxide emission does not agree with the experimental data found or with each other. Therefore an own correlation was created from experimental data. This should have the correct behavior, but the absolute values of the emissions should not be trusted.

If further improvements are to be made to the model the main focus should be on implementing the bubble phase and achieving better predictions for the emissions of sulfur dioxide and nitrogen oxide.

Although simplifications have been used, the model will work well for operator training and some optimization.

8. References

- [1] International Energy Agency. (2010) Key Energy Statistics. PDF. [Online]. http://www.iea.org/textbase/nppdf/free/2010/key_stats_2010.pdf
- [2] World Coal Association. (2012, January) Total World Electricity Generation by Fuel. [Online]. <http://www.worldcoal.org/coal/uses-of-coal/coal-electricity/>
- [3] Hartmut Spliethoff, *Power Generation from Solid Fuels*. Berlin, Germany: Springer-Verlag, 2010.
- [4] Energimyndigheten, "Energiläget 2010," 2010.
- [5] James G. Speight, *Handbook of coal analysis*. Hoboken, New Jersey, USA: John Wiley & Sons, 2005.
- [6] Simeon N. Oka, *Fluidized Bed Combustion*, E.J. Anthony, Ed. New York, USA: Marcel Dekker, Inc., 2004.
- [7] Henrik Thunman, "MEN031-Combustion Engineering," Department of Energy and Environment, Chalmers Tekniska Högskola, Göteborg, 2008.
- [8] Helmar Tepper, "Zur Vergasung von Rest und Abfallholz in Wirbelschichtreaktoren für dezentrale Energieversorgungsanlagen," Otto-von-Guericke-Universität Magdeburg, Verfahrens und Systemtechnik, Magdeburg, PhD-Thesis 2005.
- [9] Vikranth Surasani, Franka Kretschmer, Patric Heidecke, Mirko Peglow, and Evangelos Tsotsas, "Biomass Combustion in a Fluidized-Bed System: An Integrated Model for Dynamic Plant Simulations," *Industrial and Engineering Chemistry Research*, vol. 50, pp. 9936-9943, July 2011.
- [10] Peter Fritzson, *Object oriented modelling and simulation with Modelica 2.1*. New Jersey, USA: Institute of Electrical and Electronics Engineers Inc., 2004, ISBN 0-471-47163-1.
- [11] A Gomez-Barea and B. Leckner, "Modeling of biomass gasification in fluidized bed," *Progress in Energy and Combustion Science*, vol. 36, pp. 444-509, March 2010.
- [12] Yang Chen and Gon Xiaolong, "Dynamic modeling and simulation of a 410 t/h Pyroflow CFB boiler," *Computers and Chemical Engineering*, vol. 31, pp. 21-31, 2006.
- [13] M. L. de Souza-Santos, "Comprehensive modelling and simulation of fluidized bed boilers and gasifiers," *Fuel*, vol. 68, pp. 1507-1521, December 1989.
- [14] Marcio L. de Souza-Santos, *Solid Fuels Combustion and Gasification*, L. L. Faulkner, Ed. New York, USA: Marcel Dekker, 2004.

- [15] Adel F. Sarofim and Janos M. Beer, "Modeling of fluidized bed combustion," *Seventeenth Symposium (International) on Combustion*, vol. 17, pp. 189-204, 1979.
- [16] SC Saxena and GS Vogel, "The measurements of incipient fluidization velocities in a bed of coarse dolomite," *Transactions of the Institution of Chemical Engineers*, vol. 3, pp. 184-195, 1977.
- [17] CY Wen and YW Yu, "Mechanics of fluidization," *Chemical Engineering Progress Symposium*, pp. 100-125, 1966.
- [18] LH Chen CY Wen, "Fluidized bed freeboard phenomena and elutriation," *American Institute of Chemical Engineers Journal*, vol. 1, pp. 117-128, 1982.
- [19] I Tanaka, H Shinohara, H Hirose, and Y Tanaka, "Elutriation of fines from fluidized beds," *Journal of Chemical Engineering of Japan*, vol. 1, pp. 51-65, 1972.
- [20] PN Rowe and BA Partridge, "An X-ray study of bubbles in fluidized beds," *Transactions of the Institution of Chemical Engineers*, vol. 3, pp. 157-190, 1965.
- [21] DJ Gunn, "Transfer of heat and mass to particles in fixed and fluidized beds," *International Journal of Heat and Mass transfer*, vol. 4, pp. 467-492, 1978.
- [22] Prabir Basu, *Combustion and gasification in fluidized beds*, CRC Press, Ed. Boca Raton: Taylor & Francis group, 2006.
- [23] Chin-Young Wen and Max Leva, "Fluidized bed Heat transfer: A Generalized Dense-phase correlation," *American Institute of Chemical Engineering Journal*, pp. 482-488, December 1956.
- [24] SS Zabrodsky, "Heat transfer in a large particle fluidized bed with immersed in-line and staggered bundles of horizontal smooth tubes," *International Journal of Heat and Mass transfer*, vol. 4, pp. 571-579, 1981.
- [25] S. Dounit, M. Hemati, and R. Andreaux, "Modelling and experimental validation of a fluidized-bed reactor freeboard region: Application to natural gas combustion," *Chemical Engineering Journal*, vol. 140, pp. 457-465, 2008.
- [26] Subhash Mishra and Manohar Prasad, "Radiative heat transfer in participating media - a review," *Sadhana*, vol. 23, pp. 213-232, april 1998.
- [27] H.C. Hottel and E.S. Cohen, "Radiant heat exchange in gas filled enclosure: Allowance for nonuniformity of gas temperature," *American Institute of Chemical Engineering Journal*, vol. 4, pp. 3-14, March 1958.
- [28] James J. Noble, "The zone method: Explicit matrix relations for total exchange areas,"

- International Journal of Heat and Mass Transfer*, vol. 18, pp. 261-269, 1975.
- [29] K.A. Bueters and W.W. Habelt J.G. Cogoli, "Performance prediction of tangentially fired utility furnaces by computer model," *Combustion Engineering*, pp. 1245-1260, 1975.
- [30] S. Dounit, M. Hemati, and D. Steinmetz, "Natural gas combustion in fluidised bed reactions between 600 and 850C: experimental study and modelling of the freeboard," *Powder Technology*, vol. 120, pp. 49-54, 2001.
- [31] Anil K. Mehrotra, Kunal Karan, and Leo A. Behie, "Estimate gas emissivities for equipment and process design," *Chemical Engineering Progress*, pp. 70-77, September 1995.
- [32] Alireza Bahadori and Hari B. Vuthaluru, "Predicting emissivities of combustion gases," *Chemical Engineering Progress*, vol. 105, pp. 38-41, June 2009.
- [33] H. Scott Fogler, *Elements of Chemical Reaction Engineering*, 4th ed. Massachusetts, USA: Pearson Education International, 2006.
- [34] James Welty, Charles Wicks, Robert Wilson, and Gregory Rorrer, *Fundamentals of Momentum, Heat and Mass transfer*, 5th ed. USA: John Wiley & Sons, 2008.
- [35] G. van der Honing, M. Valk D. Dakic, "Fragmentation and swelling of various coals during devolatilization in a fluidized bed," *Fuel*, vol. 68, pp. 911-916, July 1989.
- [36] P. Salatino and L. Massimilla, "A descriptive model of carbon attrition in the fluidized combustion of a coal char," *Chemical Engineering Science*, vol. 40, no. 10, pp. 1905-1916, 1985.
- [37] Donald Anthony and Jack Howard, "Coal devolatilization and hydrogasification," *American Institute of Chemical Engineering Journal*, vol. 22, pp. 625-656, July 1976.
- [38] Richard Neavel, Stewart Smith, Edwin Hippo, and Robert Miller, "Interrelationships between coal compositional parameters," *Fuel*, vol. 65, pp. 312-320, March 1986.
- [39] David Merrick, "Mathematical models of the thermal decomposition of coal," *Fuel*, vol. 62, pp. 534-539, May 1983.
- [40] A. Friedl, E. Padouvas, H. Rotter, and K. Varmouza, "Prediction of heating values of biomass fuel from elemental composition," *Analytical Chimica Acta*, vol. 544, pp. 191-198, July 2005.
- [41] Sivapalan Kathiravale, Muhd Noor Muhd Unus, and K. Sopian, "Modeling the heating value of municipal solid waste," *Fuel*, vol. 82, pp. 1119-1125, June 2003.

- [42] Jose Pazo, "Biomass Thermogravimetric Analysis: Uncertainty Determination Methodology and Sampling Maps Generation," *International Journal of Molecular Science*, vol. 11, pp. 2701-2714, July 2010.
- [43] Paul Peeler and Howard Poynton, "Devolatilization of large coal particles under fluidized bed conditions," *Fuel*, vol. 71, pp. 425-430, April 1992.
- [44] F. Bustamante et al., "Kinetic of the homogeneous reverse water-gas shift reaction at high temperature," *American Institution of Chemical Engineering Journal*, vol. 50, pp. 1028-1041, 2004.
- [45] Anker Jensen et al., "Formation and reduction of NO_x in pressurized fluidized bed combustion of coal," *Fuel*, vol. 74, no. 11, pp. 1555-1569, 1995.
- [46] Anker Jensen and Jan Erik Johansson, "Modelling of NO_x emissions from pressurized fluidized bed combustion - a parameter study," *Chemical Engineering Science*, vol. 52, no. 11, pp. 1715-1731, 1997.
- [47] Jan E. Johnsson, "Formation and reduction of nitrogen oxides in fluidized bed combustion," *Fuel*, vol. 73, pp. 1398-1415, 1994.
- [48] S. Ehrlich and R.A. Chronowski, "NO_x emissions from fluidized bed boilers," *Fuel*, vol. 53, pp. 284-285, October 1974.
- [49] J. Gruhl and J.D. Teare, "Empirical models of emissions and energy efficiencies of coal fired fluidized bed power plants," MIT Energy Lab, Cambridge, 1977.
- [50] D.L. Keairns R.A. Newby, T.E. Lippert, M.A. Alvin, and D.M. Bachovchin, "Pressurized fluidized bed combustion at elevated temperatures," *Proceedings of the 10th International Conference on Fluidized Bed Combustion*, vol. 2, pp. 873-879, 1989.
- [51] J.E. Johnsson, "A kinetic model for NO_x formation in fluidized bed combustion," *Proceedings of the 10th International Conference on Fluidized Bed Combustion*, pp. 1111-1118, 1989.
- [52] Anker Jensen, Jan-Erik Johnsson, and Kim Dam-Johansen, "Nitrogen chemistry in FBC with limestone addition," *26th International Symposium on Combustion*, pp. 3335-3342, 1996.
- [53] Hakan Altindag, "Mathematical modeling of sulfur retention in fluidized bed combustors," Natural and Applied Sciences, Middle East Technical University, Turkey, Master Thesis 2003.
- [54] Hakan Altindag, Yusuf Gogebakan, and Nevin Selcuk, "Sulfur capture for fluidized bed combustion of high sulfur content lignites," *Applied Energy*, vol. 79, pp. 404-424, 2004.

- [55] M. Onur Afacan, "Mathematical modeling of NO_x emissions for bubbling fluidized bed combustors," Natural and Applied Sciences, Middle East Technical University, Turkey, Master Thesis 2005.
- [56] Ekrem Mehmet Morali, "Mathematical modeling of FBCs co-fired with lignite and biomass," Natural and Applied Sciences, Middle East Technical University, Turkey, Master Thesis 2007.
- [57] J.C Schouten and C.M. van den Bleek, "The D.U.T - SURE model: A simple approach in FBC sulfur retention modeling," *Proceedings of the 9th International Conference on Fluidized Bed Combustion*, pp. 749-761, 1987.
- [58] Weigang Lin, Peter J.M. Valkenburg, and Cor M. van den Bleek, "Prediction of NO_x and SO_x emissions in FBC of coal using easy to determine coal and sorbent characteristics," *Fuel Processing Technology*, vol. 24, pp. 399-405, 1990.
- [59] Weigang Lin, Karel Svoboda, and Cor M. van den Bleek, "Sulphur capture and its interactions with NO_x emissions in fluidized bed combustion of coal: General analytical model based on particle gas-solid reactions," *Chemical Engineering Science*, vol. 47, pp. 2425-2430, 1992.
- [60] J.C Schouten and C.M van den Bleek, "The influence of oxygen-stoichiometry on desulfurization during FBC: a simple SURE modeling approach," *Chemical Engineering Science*, vol. 43, no. 8, pp. 2051-2059, 1988.
- [61] Weigang Lin, Jianjie Bu, Rob Korbee, Karel Svoboda, and Cor M. van den Bleek, "Modeling of SO₂ and NO_x emissions in fluidized bed combustion of coal," *Fuel*, vol. 72, pp. 299-304, March 1993.
- [62] D.C Lee and C. Georgakis, "A single particle size-model for sulfur retention in fluidized bed coal combustors," *American Institute of Chemical Engineering Journal*, vol. 27, pp. 472-481, May 1981.
- [63] F. Garcia-Labiano and J. Adanez, "Characterization of the reactivity of limestones with SO₂ in a fluidized bed reactor," *The Canadian Journal of Chemical Engineering*, vol. 70, pp. 734-741, August 1992.
- [64] K.T Lee, S. Bahtia, and A.R. Mohamed, "Kinetic model for the reaction between SO₂ and coal fly ash/CaO/CaSO₄ sorbent," *Journal of Thermal Analysis and Calorimetry*, vol. 79, pp. 691-695, 2005.
- [65] K.T. Lee, K.C. Tan, I. Dahlan, and A.R. Mohamed, "Development of kinetic model for the reaction between SO₂/NO and coal fly ash/CaO/CaSO₄ sorbent," *Fuel*, vol. 87, pp. 2223-2228, 2008.

- [66] S.M. Shih, J.T. Hung, T.Y. Wang, and R.B. Lin, "Kinetics of the reaction of sulfur dioxide with calcium oxide powder," *Journal of the Chinese Institute of Chemical Engineers*, vol. 35, pp. 447-454, 2004.
- [67] J.W. Smith, "The combustion rates of coal chars, a review," *Proceedings of the 19th Symposium on combustion; The Combustion Institute*, pp. 1045-1065, 1982.
- [68] Michael Hobbs, Predrag Radulovic, and Douglas Smoot, "Modeling Fixed Bed Coal Gasifiers," *American Institute of Chemical Engineering Journal*, vol. 38, pp. 681-702, May 1992.
- [69] Normand Laurendal, "Heterogeneous kinetics of coal char gasification and combustion," *Progress in Energy and Combustion Science*, vol. 4, pp. 221-270, 1978.
- [70] Juan Adanez, Luis F. de Diego, Francisco Garcia-Labiano, Alberto Abad, and Juan C. Abanades, "Determination of biomass char combustion reactivities for FBC applications by a combined method," *Industrial and Engineering Chemistry Research*, vol. 40, pp. 4317-4323, 2001.
- [71] Charles E. Bankal, *The John Zink Combustion Handbook*, 1st ed. USA: CRC Press, 2001.
- [72] F. Johnsson, S. Andersson, and B. Leckner, "Expansion of a freely bubbling fluidized bed," *Powder Technology*, vol. 68, pp. 117-123, 1991.
- [73] S. Biyikli, K. Tuzla, and J.C Chen, "Freeboard heat transfer in high temperature fluidized beds," *Powder Technology*, vol. 53, pp. 187-194, 1987.
- [74] C. Chyang, K. Wu, and C. Lin, "Emission of nitrogen oxides in a vortexing fluidized bed combustor," *Fuel*, vol. 86, pp. 234-243, 2007.
- [75] Norra Skogsägarna. (2012, May) Grenar och toppar: Nya möjligheter för skogsägare. [Online]. <http://www.norra.se/upload/pdf-filer/skog%20broschyrer/GROT%20broschyr.pdf>
- [76] Daniel Nilsson and Sven Bernesson, "Pelletering och brikettering av jordbruksvaror: En systemstudie," Sveriges Lantbruks Universitet: Institutionen för energi och teknik, Uppsala, 2008.

Appendix I – Investigation of reaction kinetics

Models containing widely different time scales give numerical instabilities. A typical source of a fast timescale is fast kinetics. Therefore an investigation of the reaction kinetics is conducted to find what kinetics is fast enough to estimate as instantaneous. This is done using a one dimensional plug flow model of the gas phase in the bed built in Matlab. The model is isotherm, devolatilization is assumed to be instantaneous and biomass is used as fuel (using eq. (53)). Some tar is present in the inflow. The reactions and kinetics used is found in Table 3, Table 4, Table 5 and Table 9. The temperature is set to 850°C and the residence time is about 0.3 s, similar to the conditions found in a typically average bed. The char temperature is 200°C higher than the bed temperature. Two simulations are shown, one with an air to fuel ratio of about 1.2, shown in Figure 14 and one with an air to fuel ratio of about 0.4 shown in Figure 15.

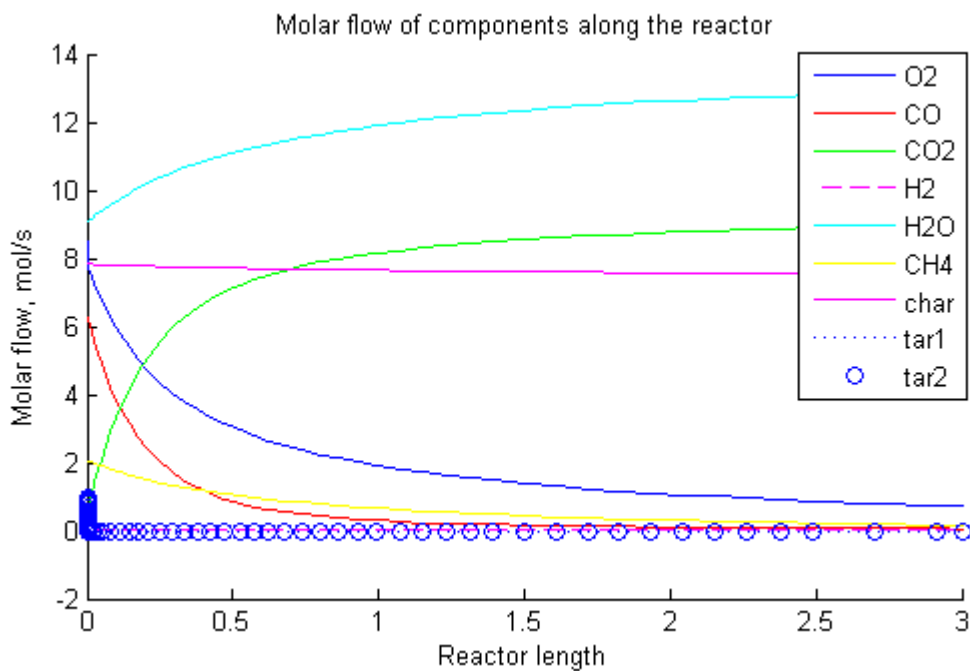


Figure 14, molar flow of each substance along a plug flow reactor with similar conditions as to the bubbling bed. The residence time is around 0.3 s. The air to fuel ratio is about 1.2.

As can be seen from Figure 15 the tar and hydrogen reactions are very fast. The char combustion is significantly slower compared to the other reactions. The carbon monoxide oxidation reaction and the methane oxidation are relatively fast.

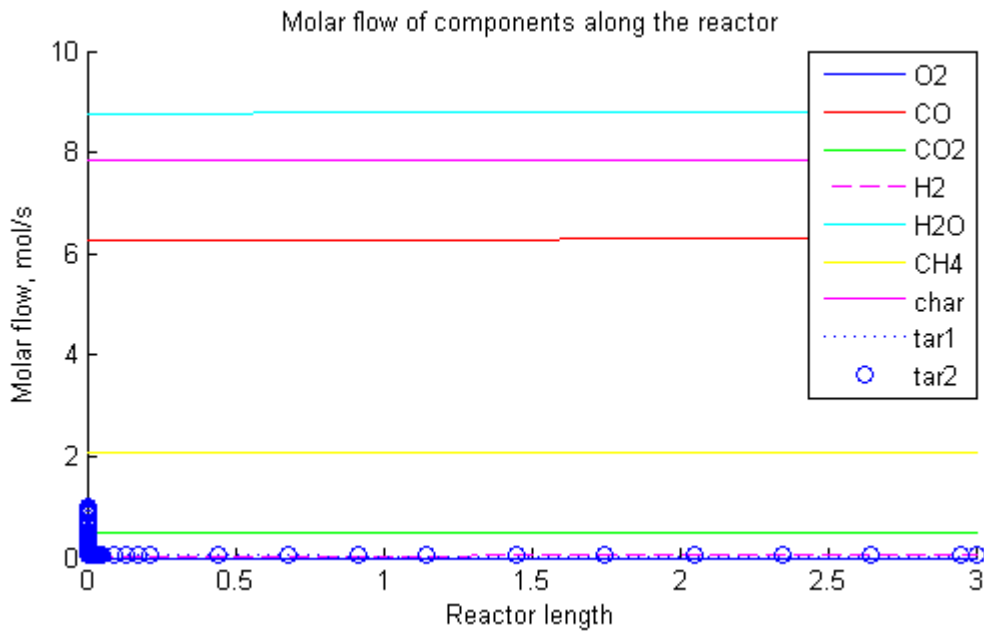


Figure 15, molar flow of each substance along a plug flow reactor with similar conditions as to the bubbling bed. The residence time is around 0.3 s. The air to fuel ratio is about 0.4.

Similar results are found in Figure 14 as in Figure 15. The char combustion rate is still significantly slower than the other reaction rates. As the air to fuel ratio is below one, both methane and carbon monoxide is present in the outlet. The outlet concentration of carbon monoxide is however significantly larger than the outlet concentration of methane, even though both of them are quite large.

From Figure 14 and Figure 15 it's clear that all reactions except for char combustion, the carbon monoxide oxidation and the methane partial oxidation can be approximated as instantaneous. As the outlet concentration of methane is low for higher air to fuel ratios and lower than carbon monoxide at the low air to fuel ratio, the partial methane oxidation is seen as instantaneous also. As the assumption of instantaneous methane partial oxidation yield a higher carbon monoxide concentration the error should not be large for air to fuel ratios not far below one for the heat and oxygen balance.

At the low air to fuel ratio shown in Figure 15 the outlet concentration is still quite large and the model may not be valid at these low air to fuel ratios. For very low air to fuel ratios the heat release in the bed will be overestimated as methane yield a higher heat output than a corresponding carbon monoxide oxidation. If the model is to be used at these low air to fuel ratios this has to be compensated for with scaling factors.

Appendix II – Freeboard radiation modeling

Radiation is one of the main heat transfer mechanisms in the freeboard area. Due to large axial temperature gradients in the gas and the presence of the hot bed the radiation modeling can be quite hard. Simulations have been conducted in Matlab using a tank in series model with a large number of tanks testing how axial radiation and bed radiation affect the temperature profile in the freeboard. The modeling of the radiation has been done according to section 3.3.4 and 4.1.2 and eq. (30) and (31) used together with tank series balances.

Figure 16 show the temperature profiles taking the different types of radiation into account. A simulation only using six tanks including bed radiation and axial radiation is also shown. The other models use 60 tanks. Radiation and convection from the specific tank volume to the wall is included in all models.

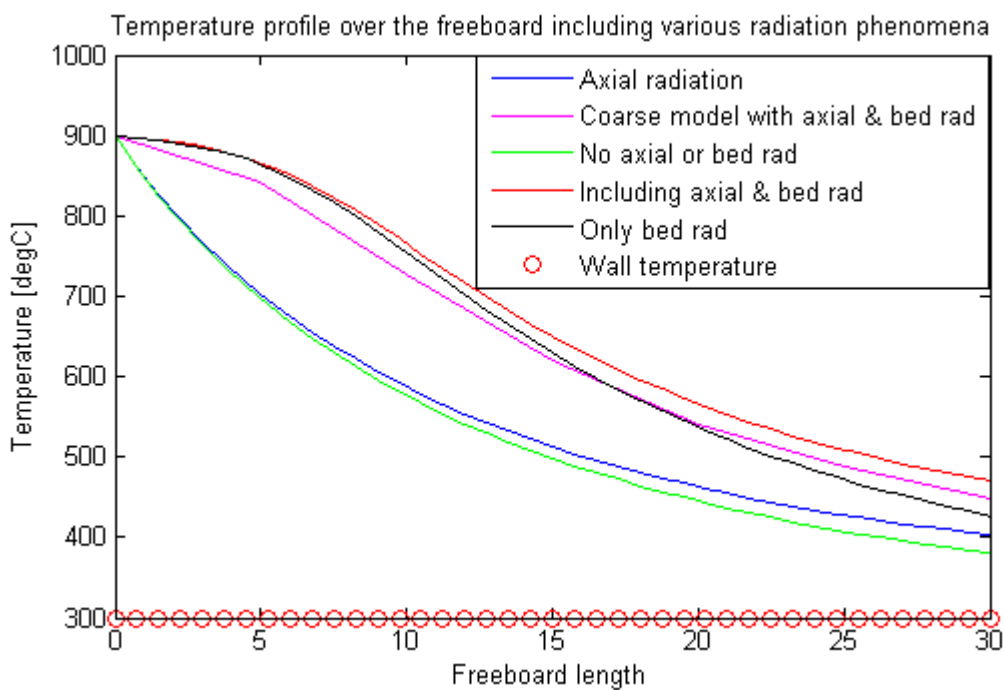


Figure 16, temperature profile over the freeboard for an cylindrical furnace with diameter of 2 m and total volume of 30 m^3 for cases with and without bed radiation and axial radiation. The bed temperature is 900°C and the wall temperature is 300°C . The purple line show the model with a smaller number of tanks.

From Figure 16 it can be seen that axial radiation has a relatively small effect on the overall temperature profile. The effect of bed radiation is however large, causing the profile to change shape. It is also clear from Figure 16 that it is possible to use a smaller number of tanks with only a smaller change in temperature profile.

Appendix III – Emission of nitrogen oxide

The formation and reduction of nitrogen oxide in fluidized bed boilers is a very complex process. The exact mechanisms are hard to find and experimental values often differ between units. This difference can often be hard to explain fully. A few things is however typical for nitrogen oxide emissions and that is that they increase with increasing temperature (even though there exist boilers showing an opposite behavior), they increase for higher air to fuel ratios and increase for higher volatile fuels [6]. From the correlation presented in eq. (57) by Newby et al. it is clear that the emissions instead decrease with increasing temperature. According to eq. (57) the emissions also increase for fuels with higher fuel nitrogen content, this is not clearly found [6] [74]. In [74] the emissions of nitrogen oxides instead decrease with increasing nitrogen content.

The correlation presented in [49] by Gruhl et al. yield lower emissions for increasing air to fuel ratio, which is not according to the experimental values found [6] [74].

From [6] it is clear that the addition of limestone to the bed has a relatively small effect on the emissions of nitrogen oxides and this effect is therefore neglected.

As no existing correlation found in literature yield correct behavior, a new simple correlation is made. The aim is to create a correlation giving correct behavior with changing fuel and combustion parameters. This type of simple correlation will not yield results accurate enough for good optimization but may give an indication to how the emission levels will change for different operating parameters.

The correlation is based on experiments found in [6]. There are various experiments presented with various coals, boilers, air to fuel ratio and temperatures. The most important parameters for the nitrogen oxide emissions are the air to fuel ratio, the temperature and the type of fuel (mainly volatile matter content). These parameters should capture the most important factors for the emission levels. The form of the correlation is presented in eq. (80). The correlation is in a form similar to eq. (57), a simple form that easily can be adapted to experimental points.

$$NO(ppm) = A \exp(-B/T) \cdot AirToFuel^C \cdot VM^D \quad (80)$$

The parameters are adapted according to the experimental data presented in Figure 17. The figure also shows the created correlation.

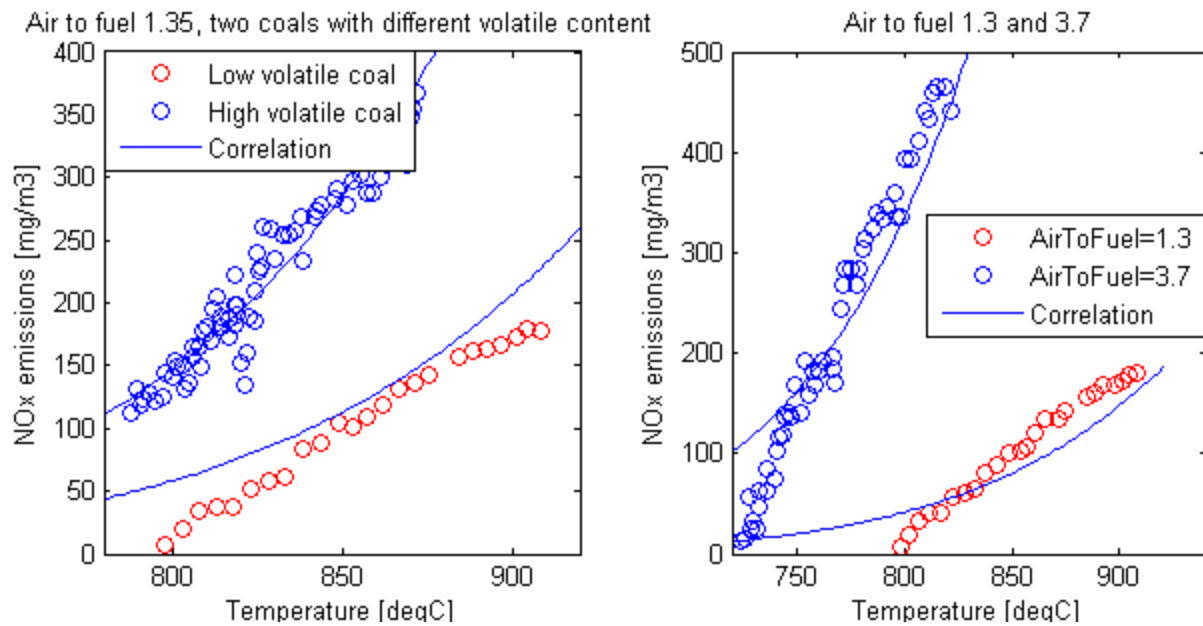


Figure 17, experimental data on nitrogen oxide emissions from bubbling fluidized bed boilers. Figure 17a show emission data correlated against temperature for two different coals. Figure 17b show emission data correlated against temperature for two different air to fuel ratios.

The final correlation is presented in eq. (81). It is clear that the exponential temperature dependence used in the correlation does not entirely fit the experimental values. The temperature dependence seems to be linear, with emissions starting to form a specific temperature. This is likely due to competing reactions reducing all formed nitrogen oxide to gaseous nitrogen or to nitrous oxide below the specific temperature. This initial temperature is hard to estimate and would have to be set for each case, so the exponential temperature dependence is considered as a good approximation.

$$NO(ppm) = 6.8 \cdot 10^8 \exp(-16 \cdot 10^3/T) \cdot AirToFuel^2 \cdot VM^{1.3} \quad (81)$$

The correlation is only valid for coals under similar conditions as those presented in the experiments. The correlation is used to capture the behavior of the nitrogen oxide emissions during variable operating conditions, the absolute values should not be trusted.

To further study the nitrogen oxide emissions an extensive kinetic model is created in Matlab based on the kinetic data in Table 6. Data on mass fractions in bed inlet, bed temperature, char content, char temperature and gas velocity in the bed are taken from the Dymola model as input values to the Matlab model.

Most preferably the data on the bubbling fluidized bed boiler used in the experiments in Figure 17 would be used, but these are not found. Therefore the data on the 16 MWth bubbling fluidized bed boiler at Chalmers is used, see Table 10. The same fuel and combustion conditions are used as those used for creating the correlation in Figure 17. Emission data from the model is assembled by conducting simulations at various bed temperatures for both fuels presented in Figure 17. The bed temperature is changed by

changing the air inlet temperature. Data for typical fuel contents in the specified coals are found in [37].

Both a plug flow model and a tank and tank series model is created of the bed and freeboard. These models yield similar results and the tank and tank series model is deemed most correct and the values from this model will be presented.

Figure 18 show the emission values from the performed simulations together with the experimental values also presented in Figure 17a.

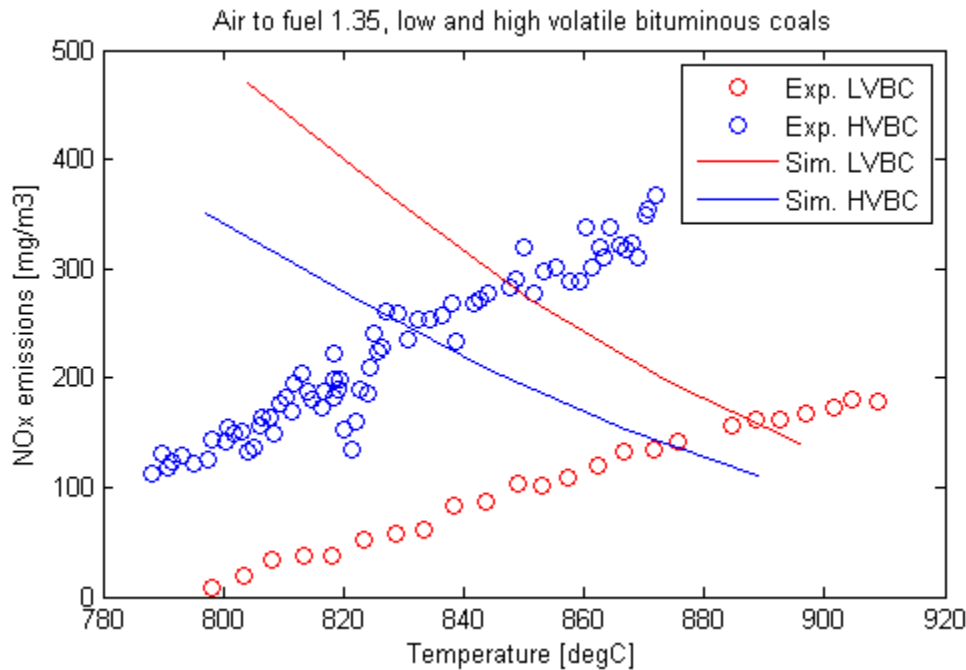


Figure 18, emission levels of nitrogen oxide from experimental values and from an extensive kinetic simulation model.

As can be seen from Figure 18 the extensive simulation model for the nitrogen oxide emission does not yield accurate results. The simulation model has a negative temperature correlation and also a negative correlation to the volatile matter content. Both these correlations are the opposite of the experimental values found.

It is interesting to note that the extensive kinetic model in its original work is used for lignite (a coal similar to the high volatile bituminous coal, blue in Figure 18) in the temperature range of 820-840°C. In this short range the model yield good emission values for the high volatile coal.

To conclude, accurate modeling of the nitrogen oxide emission is hard to achieve. Even the more extensive modeling yields inaccurate results. Therefore the simple correlation presented in eq. (81) is used in the model as an estimate. For accurate prediction of emissions from an existing boiler, experimental values from that boiler must be used.